

# A surgical window of opportunity trial evaluating the effect of the PCSK9 inhibitor evolocumab on tumoral MHC-I expression and CD8+ infiltration in glioma

**Mustafa Khasraw**

`mustafa.khasraw@duke.edu`

Duke University <https://orcid.org/0000-0003-3249-9849>

**Kirit Singh**

Duke University <https://orcid.org/0000-0002-0419-5381>

**Matthew Foster**

Duke University <https://orcid.org/0000-0003-0212-2346>

**Marlene Violette**

Duke University

**Anna Corcoran**

Duke University

**Kelly Hotchkiss**

**Chelsea Railton**

Duke University

**Emily Blandford**

Duke University

**Kathryn Blethen**

Duke University

**Elizabeth Thomas**

Duke University

**David Ashley**

Duke University <https://orcid.org/0000-0002-4754-5900>

**Annick Desjardins**

Duke University <https://orcid.org/0000-0003-3869-8283>

**Henry Friedman**

Duke University <https://orcid.org/0000-0001-7588-032X>

**Margaret Johnson**

Duke University

**Allan Friedman**

Duke University

**Stephen Keir**

Duke University

**Evan Buckley**

Duke University

**James Herndon**

Duke University

**Roger McLendon**

Duke University <https://orcid.org/0000-0001-6682-4588>

**John Sampson**

Duke University

**Evan Calabrese**

Duke University

**Giselle Lopez**

University of California San Francisco Medical Center <https://orcid.org/0000-0001-5435-6668>

**Gerald Grant**

Duke University

**Anoop Patel**

Duke University <https://orcid.org/0000-0001-7078-9535>

**Simon Gregory**

Duke University <https://orcid.org/0000-0002-7805-1743>

**Chuan-Yuan Li**

Duke University Medical Center <https://orcid.org/0000-0002-0418-6231>

**Peter Fecci**

Duke University <https://orcid.org/0000-0002-2912-8695>

---

**Article**

**Keywords:**

**Posted Date:** January 22nd, 2025

**DOI:** <https://doi.org/10.21203/rs.3.rs-5822396/v1>

**License:**  This work is licensed under a Creative Commons Attribution 4.0 International License.

[Read Full License](#)

**Additional Declarations:** **Yes** there is potential Competing Interest. MWF, MJV, KMH, COR, EEB, KEB, ELT, DMA, AD, HSF, MOJ, AF, SK, EDB, JEH, REM, EC, GAG, SGG, CYL declare that they have no competing interests. KS reports grants paid to his institution and research contracts from Adaptin Bio, which has

licensed intellectual property from Duke related to the use of Brain Bi-specific T cell Engagers (BRiTE) and combination autologous lymphocyte therapy. JHS reports an equity interest in Istari Oncology, which has licensed intellectual property from Duke related to the use of poliovirus and D2C7 in the treatment of glioblastoma. JHS is an inventor on patents related to Brain Bi-specific T cell Engagers (BRiTE), PEP-CMV DC vaccine with tetanus, as well as poliovirus vaccine and D2C7 in the treatment of glioblastoma. GYL reports consulting fees from Servier Pharmaceuticals. GYL is a consultant for and has equity in SNPsnipe, Inc. APP is a consultant for Sygnomics, Syapse, and Servier Pharmaceuticals, and has an equity in Sygnomics. PEF reports support as an Akash fellow of the CRI Lloyd J. Old STAR award program and has received consulting fees and grant funding from Monteris Medical outside the submitted work. MK reports grants or contracts from BMS, AbbVie, BioNTech, CNS Pharmaceuticals, Daiichi Sankyo Inc., Immorna Therapeutics, Immvira Therapeutics, JAX lab for genomic research, and Personalis, Inc.; received consulting fees from AnHeart Therapeutics, Berg Pharma, George Clinical, Manarini Stemline, and Servier; received honoraria from GSK; and is on a data safety monitoring board for BPG Bio.

---

# A surgical window of opportunity trial evaluating the effect of the PCSK9 inhibitor evolocumab on tumoral MHC-I expression and CD8<sup>+</sup> infiltration in glioma

**Authors:** Kirit Singh<sup>1,2</sup>, Matthew W. Foster<sup>3</sup>, Marlene J. Violette<sup>3</sup>, Anna M. Corcoran<sup>1,2</sup>, Kelly M. Hotchkiss<sup>1,2</sup>, Chelsea O. Railton<sup>1,2</sup>, Emily E. Blandford<sup>1,2</sup>, Kathryn E. Blethen<sup>1,2</sup>, Elizabeth L. Thomas<sup>1,4</sup>, David M. Ashley<sup>1</sup>, Annick Desjardins<sup>1</sup>, Henry S. Friedman<sup>1</sup>, Margaret O. Johnson<sup>1</sup>, Allan Friedman<sup>1,2</sup>, Stephen Keir<sup>1</sup>, Evan D. Buckley<sup>6</sup>, James E. Herndon<sup>5,6</sup>, Roger E. McLendon<sup>1,4</sup>, John H. Sampson<sup>1,2</sup>, Evan Calabrese<sup>7</sup>, Giselle Y. Lopez<sup>1,2,4</sup>, Gerald A. Grant<sup>1,2</sup>, Anoop P. Patel<sup>1,2</sup>, Simon G. Gregory<sup>1,2</sup>, Chuan-Yuan Li<sup>8</sup>, Peter E. Fecci<sup>1,2†</sup>, Mustafa Khasraw<sup>1,2†\*</sup>

## Affiliations:

<sup>1</sup>The Preston Robert Tisch Brain Tumor Center at Duke University; Durham, NC, US.

<sup>2</sup>Department of Neurosurgery, Duke University; Durham NC, US.

<sup>3</sup>Duke Proteomics and Metabolomics Core Facility, Duke University; Durham, NC, US.

<sup>4</sup>Department of Pathology, Duke University; Durham, NC, US.

<sup>5</sup>Department of Biostatistics and Bioinformatics, Duke University; Durham, NC, US.

<sup>6</sup>Duke Cancer Institute Biostatistics, Duke University; Durham NC, US.

<sup>7</sup>Department of Radiology, Duke University; Durham, NC, US.

<sup>8</sup>Adjunct Professor in the Department of Dermatology, Duke University; Durham, NC, US.

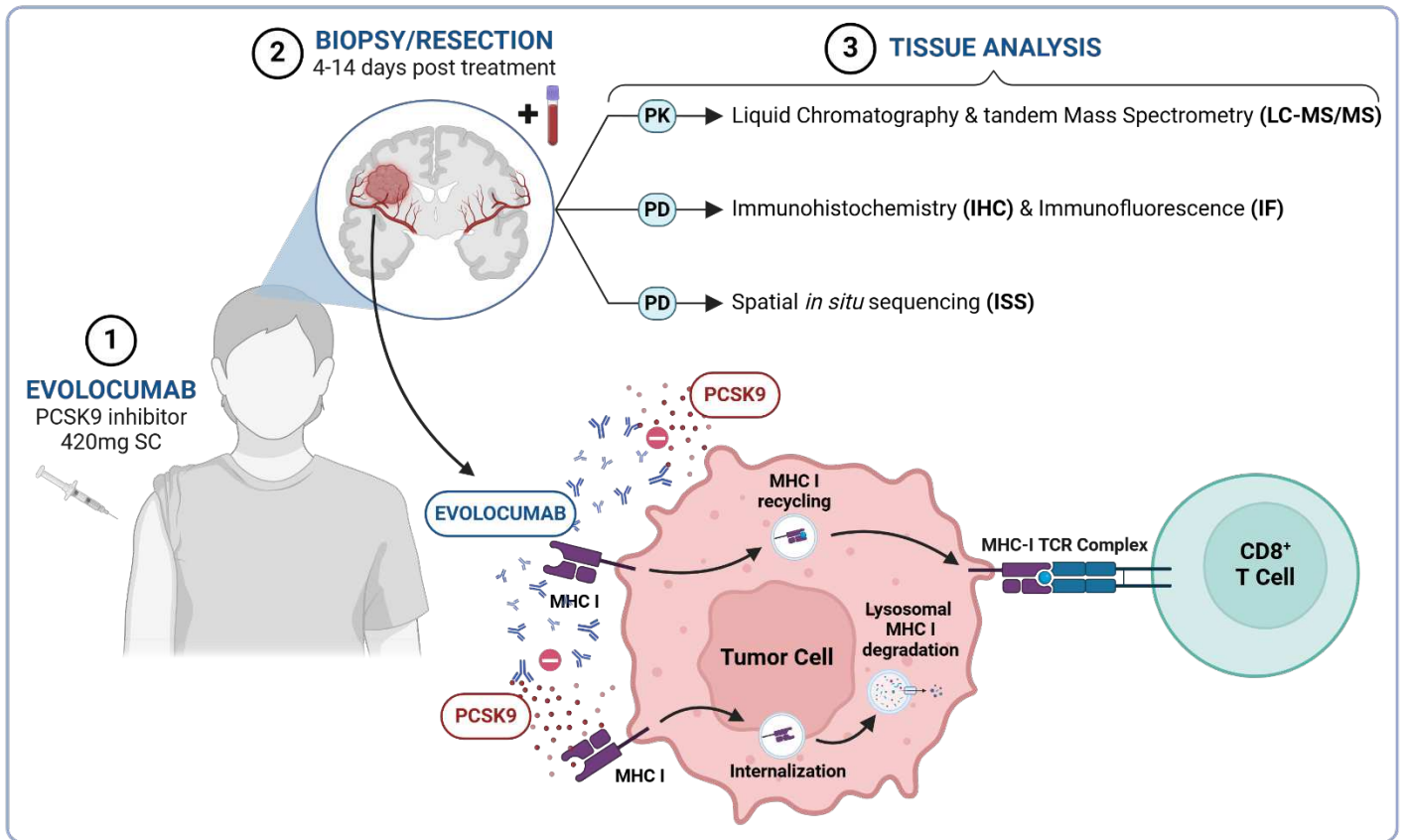
<sup>†</sup>These authors contributed equally to the manuscript.

**\*Corresponding Author.** Mustafa Khasraw, MD, The Preston Robert Tisch Brain Tumor Center, Duke University | Box 3624, Durham, NC 27710, T +1 919.684.6173 | F +1 919.681.1697, [mustafa.khasraw@duke.edu](mailto:mustafa.khasraw@duke.edu)

**Abstract:** Many cancers evade immunosurveillance by downregulating surface major histocompatibility class (MHC)-I. Proprotein convertase subtilisin/kexin type 9 (PCSK9) promotes MHC-I degradation and is elevated in glioma. Evolocumab is a clinically approved PCSK9 inhibitor, which restores MHC-I expression in pre-clinical cancer models. However, monoclonal antibodies (mAbs) have limited blood brain/tumor barrier penetrance (BBB/BTB). The aim of this window-of-opportunity trial was to evaluate evolocumab's BBB/BTB penetrance and biological effect in glioma (PesKE; NCT04937413). Patients with newly diagnosed/recurrent glioma undergoing a clinically indicated biopsy or resection were enrolled (n=32, M: 16, F: 16; control average age: 51.85, evolocumab: 53). Intervention participants (n=6) received subcutaneous evolocumab 4-14 days pre-procedure. 4/6 intervention participants provided research tissue. No significant adverse events were observed. Evolocumab was detected in all analyzed intervention tissue, with an average tumor:blood ratio of 0.0222 (SD±0.0190), akin to other mAbs. Evolocumab quantitation was 4.44x greater in contrast-enhancing (mean 0.0068 fmol/mcg (SD±0.001)) vs non-contrast enhancing cases (mean 0.0015 fmol/mcg (SD±0.0004)). Proteomic analysis found positive trends between evolocumab and MHC-I subtypes (HLA-A-C, E-G), with a significant positive correlation with HLA-H (R<sup>2</sup>=0.9584, p=0.021\*). Tumor tissue with higher evolocumab titers demonstrated increased surface MHC-I and CD8<sup>+</sup> T cell infiltration. Increased CD8<sup>+</sup> *TNF*, *FASLG* and *GZMA* transcription was observed in high titer tissue compared to low titer tissue/untreated controls. Pre-resection evolocumab is well tolerated but exhibits BBB/BTB penetrance akin to other mAbs. Increased tumoral evolocumab/PCSK9i may enhance tumoral MHC-I/effector CD8<sup>+</sup> infiltration. Future work will explore combining evolocumab with BBB/BTB opening therapies like low-intensity focused ultrasound.

**One Sentence Summary:** We conducted a tissue-based study in glioma patients to evaluate if peripheral evolocumab enters tumors, enhances surface MHC-I, and boosts effector CD8<sup>+</sup> T cell infiltration.

# Graphical Abstract



# Main Text:

## INTRODUCTION

Tumoral evasion of the immune system is a key driver of resistance to immunotherapy. One such method of evasion is downregulation of surface major histocompatibility complex class I (MHC-I)<sup>1</sup>. Absence of MHC-I restricts neoantigen presentation and conceals tumors from cytotoxic CD8<sup>+</sup> T cells<sup>2</sup>. This phenomenon has been observed in many cancers, including primary brain malignancies, which are typically immunologically cold and possess few tumor-infiltrating lymphocytes (TILs)<sup>3</sup>. While recent findings by our group demonstrate that CD8<sup>+</sup> killing of tumor can occur independently of MHC-I via the NKG2D-NKG2DL axis<sup>4</sup>, such killing depends on prior T cell priming via T cell receptor (TCR) activation. Restoring MHC-I expression may facilitate this priming of CD8<sup>+</sup> T cells, enhancing anti-tumor effect<sup>5</sup>.

*Liu et al* recently demonstrated that proprotein convertase subtilisin/kexin type 9 (PCSK9), a regulator of cholesterol metabolism, also influences the recycling of MHC-I receptors between the plasma membrane and cytoplasm<sup>6</sup>. While PCSK9 was initially identified as a drug target for hypercholesterolemia owing to its degradation of the low-density lipoprotein receptor (LDL-R)<sup>7</sup>, it has subsequently been shown to affect several other surface receptors including the very low-density lipoprotein receptor (VLDL-R), Apolipoprotein E receptor 2 (ApoER2) and cluster of differentiation 36 receptor (CD36)<sup>7,8</sup>. In a similar fashion, *Liu et al* reported that PCSK9 promotes the internalization of MHC-I within intracellular lysosomes, wherein it is degraded<sup>6</sup>. Deletion/inhibition of PCSK9 blocks this process, resulting in increased tumoral MHC-I expression (mechanism in **graphical abstract**). This finding holds potential therapeutic implications, as *Liu et al* also reported that PCSK9 inhibition (PCSK9i) could potentiate the effect of immune checkpoint blockade (ICB, specifically anti-programmed-death 1 ( $\alpha$ PD-1)) against murine models of colon cancer and melanoma<sup>6</sup>.

Notably, interrogation of the pan-cancer cohort within the human protein atlas finds that circulating plasma PCSK9 levels are increased in patients with glioma compared to other malignancies (**Fig. 1**)<sup>9</sup>. Having previously outlined the need for combination immunotherapies to overcome high-grade gliomas resistance to multiple therapies<sup>10</sup>, we considered whether PCSK9 might be a druggable target in the context of primary brain malignancy. We hypothesized that PCSK9i could reduce MHC-I degradation in glioma, thereby enhancing the infiltration and activity of CD8<sup>+</sup> lymphocytes. PCSK9i could then be considered as part of a future combination approach with T cell dependent therapies like ICB.

Such an approach would benefit from the commercial availability of PCSK9i therapies, which are approved by the Food and Drug Administration (FDA) for the management of hypercholesterolemia<sup>11,12</sup>. Therapies include the monoclonal antibodies alirocumab<sup>13</sup> and evolocumab<sup>14</sup> as well as the small interfering RNA (siRNA) inclisiran<sup>15</sup>. For this study, we elected to evaluate evolocumab as it had been used to demonstrate anti-tumor efficacy in combination with  $\alpha$ PD-1 ICB by *Liu et al*. Evolocumab also has a well-established safety profile, with the most common reported adverse event being mild injection-site reactions<sup>11</sup>. Further, at the maximum dose of 420 mg, evolocumab rapidly decreased unbound PCSK9 in the periphery within 4 hours of administration and fully suppressed PCSK9 levels up to 14 days following a single treatment<sup>16</sup>. However, as a monoclonal antibody (mAb), we were uncertain whether evolocumab could cross the blood-brain/tumor barrier (BBB/BTB) in sufficient quantities to exert a biological effect<sup>17</sup>. Although the BBB/BTB becomes disrupted in glioma (via surgery, radiotherapy, or disease progression), regions of tumor may remain inaccessible behind non-disrupted BBB/BTB<sup>18</sup>. Despite this, evaluations of peripherally administered mAb therapy in the context of

high-grade glioma ( $\alpha$ PD-1) have demonstrated biological effect in the central nervous system (CNS) despite a cerebral-spinal fluid (CSF):serum ratio of just 0.009<sup>19</sup>. Further, evolocumab could feasibly associate with unbound PCSK9 in the periphery, thereby preventing its effect on tumor MHC-I expression within the CNS.

Our aims therefore were to determine whether peripheral evolocumab could be detected in the tumors of glioma patients, and whether this would be in sufficient quantities to increase surface MHC-I with resultant infiltration of cytotoxic CD8<sup>+</sup> lymphocytes. To do so, we conducted a surgical window of opportunity study – The PCSK9i Inhibitor Evolocumab: A Surgical Trial of Pharmacodynamics and Kinetics Evaluation (PesKE, NCT04937413). The primary objective of this trial was to evaluate whether evolocumab could cross the BBB/BBB and be detectable in intracranial glioma following subcutaneous administration. Secondary objectives included (1) determining the uptake ratio of evolocumab into the CNS by comparing levels in tumor vs blood and (2) evaluating the downstream effects of PCSK9i on tumoral MHC-I abundance/expression and lipid metabolism. Exploratory analyses included evaluating changes in the characteristics of infiltrating immune cells between both groups. Safety monitoring for adverse events when using evolocumab in the context of glioma was also conducted throughout. We report our findings and outline potential approaches for using PCSK9 inhibition as part of a combination strategy to treat intracranial malignancies.

## RESULTS

### Peripheral high-dose evolocumab is well tolerated in patients undergoing biopsy/resection of glioma

A total of 32 adult participants ( $\geq 18$  years old) with newly diagnosed or recurrent glioma consented to enroll on study (16M, 16F) between October 2021 and June 2023. Of the 32 patients recruited to the study, 6 participants received evolocumab treatment (average age 53 (SD $\pm$ 19.88)), while 26 were assigned to the non-treatment group (average age 51.85 (SD $\pm$ 16.07)). Full demographics and a breakdown of the diagnoses for both groups, including whether participants had newly diagnosed or recurrent glioma, is shown in **Table S2**). Tissue was taken for research if excess was available beyond that required for diagnostic purposes.

Of participants enrolled in the treatment arm, 5 patients proceeded to surgical resection/biopsy of their tumor. One treatment patient was not able to proceed to surgical resection. Four of the 5 treated patients who underwent resection had both post-treatment blood and tumor tissue available for analysis for the primary outcome. In the control arm, 17 participants had sufficient tissue and blood available for comparison (CONSORT<sup>20</sup> flowchart showing tissue distribution shown in **Fig. 2**). Time from treatment with evolocumab to tumor resection was 4.4 days on average (SD $\pm$ 1.5). Over the course of the study, no grade 3-5 adverse events (AEs) or serious adverse events (SAEs) were recorded. The commonest were injection site reactions of the mild-moderate adverse events that were possibly, probably, or definitely related to evolocumab (n=2 (33%)). A summary of all adverse events recorded during this study is shown in **Table S3** with those possibly, probably, or definitely related to evolocumab shown in **Table S4**.

### Peripherally administered evolocumab is detected in intracranial tumors, with enhanced titers in contrast-enhancing disease

To detect evolocumab accurately and specifically in tumor, we used liquid chromatography coupled to tandem mass spectrometry (LC-MS/MS). We selected three candidate “proteotypic” tryptic peptides after analysis of neat drug based on uniqueness versus reference human proteomes<sup>21</sup> and validated these using drug after spiking into pooled human plasma. Evolocumab was quantified via a targeted LC-MS/MS assay that used stable isotope-labeled (SIL) internal standard peptides and an external calibration curve<sup>22</sup>. Using peptides which gave best figures-of-merit (i.e., lowest limits of detection and quantification), evolocumab was below limit of detection in blood prior to treatment but was quantified in all intervention patients following administration of drug, confirming specificity of detection (p=0.0286\*, two-tailed Mann-Whitney U test, **Fig. 3A**). On evaluating tumor tissue, we were able to detect drug in all analyzed intervention cases, with minimal background signal observed in control tissue (intervention vs control arm; mean evolocumab quantitation of 0.0045 fmol/mcg (SD $\pm$ 0.0038) vs  $1.4594 \times 10^{-5}$  fmol/mcg (SD $\pm$ 2.6654  $\times 10^{-5}$ ) respectively, p=0.0015\*\*, **Fig. 3B**). A positive, albeit non-significant, relationship was observed between evolocumab titers in blood and evolocumab titers in tumor (R<sup>2</sup>=0.4020, p=0.2663, Pearson’s Correlation Coefficient, **Fig. 3C**). The average tumor: blood ratio of evolocumab was 0.0222 (SD $\pm$ 0.0190)), similar to other peripherally administered monoclonal antibodies (mAbs, aPD-1: 0.009<sup>19</sup>).

Increased tumoral evolocumab titers were detected in intervention cases 1004 and 1007, with lower titers in cases 1005 and 1008 (**Fig. 3D**). Evaluation of pre-operative imaging and pathology for the two cases with lower evolocumab titers found that they were low grade non-contrast enhancing tumors (ID 1005: grade III Oligodendroglioma, ID 1008: grade II Astrocytoma, average evolocumab detection of 0.0015 fmol/mcg (SD $\pm$ 0.0004), magnetic-resonance imaging (MRI) sequences shown in **Fig. 4A-D**). Conversely, cases with higher evolocumab titers were grade IV glioblastomas, with evidence of contrast enhancement on MRI imaging (IDs: 1004 & 1007, average evolocumab detection of 0.0068 fmol/mcg (SD $\pm$ 0.001), 4.44x compared to non-contrast cases). Though we had observed a positive relationship between levels of evolocumab in blood and levels of evolocumab in tumor, we noted that the greatest

tumor: blood ratio was not in the case with the highest drug quantitation, but instead in the case with the greatest degree of contrast enhancement (ID: 1004, tumor: blood ratio of 0.0547, T1-post contrast MRI sequence shown in upper right quadrant of **Fig. 4C**). We concluded that while subcutaneously administered evolocumab entered CNS tumor tissue, overall uptake was similar to other monoclonal antibodies, with greater entry into tumors with greater BBB/BBB disruption.

### **Higher evolocumab uptake in tumor is associated with increased MHC-I and decreased Apolipoprotein E quantities within the tumor proteome**

We next sought to evaluate the biological effect of evolocumab on tumor. We hypothesized that drug treatment would result in increased MHC-I levels in resected/biopsied tissue. To measure MHC-I levels, we initially anticipated using flow cytometry. However, limited tissue volumes from biopsy samples required us to use less tissue-intensive methods, and we therefore performed non-targeted tumor proteome analysis via LC-MS/MS on samples used for initial drug quantitation. First, we began by evaluating if non-targeted LC-MS/MS could appropriately determine high or low MHC-I expression on glioma cells. To do so, we analyzed immortalized glioma lines that have been reported in the literature to express either high levels of MHC-I (U343MG, MHC-I<sup>Hi</sup>) or lower levels of MHC-I (U87MG, MHC-I<sup>Lo</sup>)<sup>23</sup>. We confirmed the relative expression of MHC-I (HLA-ABC) via flow cytometric analysis (**Fig. 5A**) before analyzing the same cell lines via LC-MS/MS. Similar trends in relative levels of HLA-A, -B and -C were quantified in the cell proteomes from tryptic digests by non-targeted proteomics, with higher levels observed in the MHC-I<sup>Hi</sup> U343MG versus MHC-I<sup>Lo</sup> U87MG line (**Fig. 5B**). These data validated the use of LC-MS/MS for quantification of relative MHC-I.

Subsequent clinical sample analysis of all MHC-I subtypes via LC-MS/MS revealed positive trends between the amount of Evolocumab in tumor and quantified protein levels of HLA-A (**Fig. 5C**), HLA-B (**Fig. 5D**), HLA-E (**Fig. 5F**), HLA-F (**Fig. 5G**) and HLA-G (**Fig. 5H**, non-targeted proteomic data only available for 2/4 cases), though these correlations were non-significant. We did, however, observe a significant positive correlation between Evolocumab and HLA-H in tumor ( $R^2=0.9584$ ,  $p=0.021^*$ , Pearson's Correlation Coefficient, **Fig. 5I**). Overall, broadly similar trends across MHC-I subtypes and evolocumab levels were observed, with the exception of HLA-C which remained unchanged (HLA-C shown in **Fig. 5E**, trends across all subtypes shown in **Fig. 5J**).

We next evaluated if increased evolocumab levels in tumor also resulted in changes in lipid pathways within the brain. On reviewing the non-targeted proteomic analysis for relevant markers, we first considered PCSK9 itself. However, LC/MS-MS quantitation of PCSK9 was incomplete for intervention samples, precluding analysis. We instead reviewed other regulators of lipid metabolism with the CNS. Noting that PCSK9 has been implicated in the degradation of Apolipoprotein E (ApoE) receptors, and that ApoE is the major apolipoprotein regulating CNS lipid metabolism<sup>24</sup>, we analyzed relative ApoE abundances. Non-targeted proteomic data was available for ApoE levels in all intervention cases. We hypothesized that evolocumab would prevent degradation of ApoE receptors<sup>7</sup> and therefore decrease ApoE protein levels. Indeed, we observed a significant negative correlation between ApoE protein levels and intratumoral evolocumab ( $R^2=0.9113$ ,  $p=0.0454^*$ , **Fig. 5K**). Together, these data were indicative of greater biological effect within tumors as drug uptake increased.

## Increased cytotoxic CD8<sup>+</sup> T cell infiltration and MHC-I cell surface expression is observed near proliferating tumor cells in tissue with higher evolocumab titers

Finally, we sought to establish whether the increased MHC-I abundance in the proteome reflected increased expression on tumor. To do so, we performed parallel spatial *in situ* sequencing (ISS), immunofluorescence (IF), and immunohistochemistry (IHC) in tumor tissue with either lower (ID: 1008) or higher (ID: 1007) evolocumab uptake. Using ISS and H&E staining, we classified various cell subtypes using canonical genes and identified regions of tumor, including proliferating (Ki-67<sup>Hi</sup>) malignant cells (exemplar ID: 1007 in **Fig. 6A**, niches in **Fig. 6B**, Ki-67<sup>Hi</sup> tumor cells and CD8<sup>+</sup> lymphocytes shown in **Fig. 6C**, clustering analysis and identification in **Fig. S2-3**, H&E in **Fig. S4**).

Interestingly, ISS revealed transcriptional evidence of focal parenchymal aggregates of CD8<sup>+</sup> lymphocytes throughout tumor tissue with high evolocumab uptake, including adjacent to proliferating tumor cells (**Fig. 6C**, CD8<sup>+</sup> cells highlighted in red, Ki-67<sup>Hi</sup> tumor cells indicated with purple arrows). Unblinded pathologist review also identified parenchymal aggregates of CD8<sup>+</sup> cells in IHC staining of the same tissue, noting that this behavior differed from the typical perivascular pattern seen in glioma. Curious as to whether this increased CD8<sup>+</sup> infiltration correlated with changes in MHC-I, we conducted a focused IF analysis of the area where ISS/IHC labelled CD8<sup>+</sup> aggregates were seen adjacent to proliferating tumor cells. In these regions, we observed high MHC-I expression via IF, which notably overlapped with the membrane marker Wheat Germ Agglutinin (WGA, focused CD8<sup>+</sup> IHC sequence in **Fig. 6D**, paired focused IF of DAPI, GFAP, MHC-I and WGA in **Fig. 6E & 6F**). Similar trends were not seen in tumor tissue with lower evolocumab uptake, where sparse CD8<sup>+</sup> infiltration on ISS/IHC and reduced co-membranous MHC-I expression was seen (paired ISS, CD8<sup>+</sup> IHC and MHC-I IF in **Fig. S5**, H&E in **Fig. S6**).

Having observed enhanced CD8<sup>+</sup> infiltration adjacent to proliferating tumor cells, we next considered the functional status of these lymphocytes. CD8<sup>+</sup> activity across the whole sample was compared between untreated controls, low evolocumab uptake tissue and high evolocumab uptake tissue using ISS. Comparisons were made via transcriptomic analysis using canonical markers of effector T cell activity (*GZMB*, *IFNG*, *TNF*, *FASLG*, *PRF1*, *GZMK*, *GZMA*) (**Fig. 6G**). For tissue with high evolocumab uptake, transcriptional levels of the cytotoxic genes *TNF*, *FASLG* and *GZMA* were increased above levels in both untreated controls and low evolocumab uptake tissue (evolocumab high vs non-treated % CD8<sup>+</sup>: *TNF* 2.78x, *FASLG* 2.62x, *GZMA* 1.89x, **Fig. 6H**). We also evaluated the transcription of T cell exhaustion genes (*PDCD1*, *FOXP3*, *LAG3*, *CTLA4*, *TOX*, *TIGIT*) and observed increases of these markers compared to untreated and low drug uptake samples (**Fig. 6I**). Taken together, these data suggested increased cell surface expression of MHC-I in tumor tissue with high evolocumab uptake, accompanied by parenchymal CD8<sup>+</sup> infiltration and evidence of effector T cell activity.

## DISCUSSION

Immunologically cold tumors like high-grade gliomas have proven resistant to immunotherapies such as immune checkpoint blockade<sup>26</sup>. Loss of MHC-I has long been considered to be a key factor in resistance to immunotherapy, although recent findings by our group demonstrate that CD8<sup>+</sup> killing can occur independently of MHC-I via the NKG2D-NKG2DL axis<sup>4</sup>. However, such killing depends on prior TCR activation and restoring MHC-I expression may also facilitate this priming of CD8<sup>+</sup> anti-tumor activity.

We performed a small-scale tissue-based trial to assess both the pharmacokinetics and pharmacodynamics of evolocumab in glioma – a drug that has been shown to increase MHC-I expression and potentiate ICB in other cancers *in vivo*. We report that evolocumab appears to have PK characteristics (i.e., BBB/BTB penetrance) in keeping with other mAbs that have not demonstrated efficacy against glioblastoma<sup>19,26</sup>. However, we did observe PD changes (i.e., biological activity) that correlated with levels of intratumoral evolocumab. Across the majority of MHC-I subtypes, we observed positive relationships between intratumoral drug levels and proteomic quantitation of HLAs, with a significant positive correlation between intratumoral evolocumab and HLA-H. Interestingly, while HLA-H was initially characterized as a non-functional pseudogene<sup>27</sup>, recent findings suggest evidence of transcriptional activity<sup>28</sup> including roles in mobilizing other HLA subtypes to the cell surface<sup>29</sup>. Subsequent analysis via paired spatial ISS/IHC/IF found that tumor tissue with high evolocumab uptake demonstrated high levels of membranous MHC-I expression. These regions of high membranous MHC-I co-localized with parenchymal CD8<sup>+</sup> infiltration, an uncharacteristic finding in higher-grade gliomas<sup>30,31</sup>.

Further correlative evidence of increased biological activity was demonstrated by the significant inverse relationship between intratumoral evolocumab and levels of ApoE, a key regulator of CNS lipid metabolism (ApoE<sup>24</sup>). As mentioned previously, evolocumab has been shown to prevent loss of the ApoER2 receptor<sup>7</sup>, which internalizes and promotes the degradation of ApoE. This observed effect of evolocumab reducing ApoE levels in the CNS may also be of value, given that ApoE is over-expressed in high and low-grade gliomas<sup>32</sup>. In particular, ApoE induces immunosuppressant signaling in the CNS<sup>33</sup> including the polarization of macrophages from a pro-inflammatory M1 to an anti-inflammatory M2 phenotype<sup>34,35</sup>. Given that immunosuppressive tumor associated macrophages (TAMs) are abundant in high-grade gliomas<sup>36</sup>, this effect would likely be beneficial in promoting a more efficacious anti-tumor immune response. Therapeutic targeting of ApoE and its isoforms in the CNS may also be of value in other disease areas, including neurodegenerative diseases, such as Alzheimer's<sup>37,38</sup>.

Despite these promising findings, our study is limited by the small sample size of the treatment arm, with analysis of relationships between intratumoral evolocumab and PD parameters such as MHC-I subtypes/ApoE limited to just 4 cases. This limitation was likely caused by the trial design, where patients were offered a single dose of evolocumab only, potentially reducing interest in the study. Future tissue-based studies will benefit by offering sustained therapeutic intervention after tissue acquisition to facilitate patient enrollment. Another potential confounder for interpreting our findings include the potential of peripheral blood contamination in surgically acquired tissue samples. This is particularly problematic when attempting to detect low levels of drug in small amounts of tissue (as will likely be the case in many surgical window of opportunity studies conducted in the CNS). While there are processes to minimize cross contamination, ranging from the simple (e.g., rinsing tissue with saline to remove excess blood, as was performed in this study) to complex (normalization to quantitated hemoglobin protein levels in tissue and blood), there is little validation regarding the relative efficacy of these. Ultimately, standardized processes to assess drug quantitation and biological effect are required. This will require harmonization of approaches to remove confounding drug signal from peripheral blood and agreed LC-MS/MS protocols for quantitation of protein levels in tissue.

Nevertheless, small-scale Window of Opportunity studies afford us the ability to quickly assess the impact of treatment. Given the suggestion of increased PD effect with greater PCSK9i in tumor, but PK characteristics of evolocumab that are similar to other mAbs, we could rationalize early modification of our treatment approach based on these initial findings. Modifications may include combination alongside modalities that increase the uptake of larger constructs into the brain such as low-intensity focused ultrasound (LIFU) via transient BBB/BTB opening<sup>39,40</sup> or lipid nanoparticle encapsulation of PCSK9 siRNA<sup>41</sup> to aid BBB/BTB penetration. Notably, we observed increased transcription of markers associated with both cytotoxicity and exhaustion in CD8<sup>+</sup> T cells which entered tumor tissue with high evolocumab uptake. A combination strategy leveraging BBB/BTB opening to facilitate the entry of therapies that upregulate MHC-I and prevent exhaustion (i.e., ICB) may further enhance intra-tumoral CD8<sup>+</sup> T cell activity.

In conclusion, pre-operative high dose evolocumab in patients undergoing resection or biopsy for glioma appears to be well tolerated. However, the uptake of evolocumab across the BBB/BTB is in keeping with other antibody therapies, with the highest uptake observed in cases with the greatest degree of contrast-enhancement. Despite this, we find suggestions of mechanistic effect of PCSK9i in the context of high-grade glioma. Increases across the majority of MHC-I subtypes and decreases in ApoE levels were observed as intratumoral evolocumab titers rose. In tumor tissue with high evolocumab uptake, concomitant cell surface MHC-I expression and CD8<sup>+</sup> T cell infiltration was observed. Future work will explore combination strategies that can enhance evolocumab uptake into high-grade gliomas, including low-intensity focused ultrasound and the addition of ICB therapies to prevent infiltrating CD8<sup>+</sup> T cell exhaustion.

## **MATERIALS AND METHODS**

### **Study oversight and design**

PesKE was a non-randomized, open-label, single-center surgical window of opportunity study. This study recruited adult patients ( $\geq$  18 years old) with newly diagnosed or recurrent glioma and who had a clinical indication for either gross macroscopic resection, debulking, or biopsy of their disease. Participants were enrolled if pre-operative imaging indicated a sufficient tumor size that would allow for collection of specimens for the required analyses. A full list of final eligibility criteria is included in **Table S1**.

Once enrolled, participants on the treatment arm received 420mg of Evolocumab (administered subcutaneously) 4-14 days prior to their surgical procedure. Participants were assigned to the treatment arm if it was logistically feasible for them to receive subcutaneous evolocumab prior to their planned procedure (i.e., patients could attend for pre-operative administration of drug within the study's timeframe of 4-14 days prior to procedure). Participants assigned to the control arm received no treatment prior to surgery. All participants enrolled in the study were assigned to have an intra-operative blood draw at the time of tissue collection. Treatment patients also underwent a blood draw prior to evolocumab administration. Tumor tissue for research purposes was only taken after sufficient tissue for clinical diagnostic purposes was collected. Participants on the treatment arm were then followed up for two weeks following surgery or biopsy and monitored for adverse events as well as routine post-operative assessments of physical and neurological status as well as standard laboratory evaluations. An overview of the study design is shown in **Fig. S1**.

The study received approval by the institutional review board at the Duke Cancer Institute (DCI, Duke IRB# Pro000108375), and was conducted at the same center. The study was registered on ClinicalTrials.gov (NCT04937413) on June 16th, 2021, and the first patient was enrolled on October 18th, 2021. The study was completed on June 21st, 2024. Study monitoring was performed both internally by the Principal Investigator (PI) and institutionally by the DCI. Audits of compliance with the protocol and principles of Good Clinical Practice were routinely performed by the Duke Office of Audit, Risk and Compliance (OARC). Data and Safety Monitoring were performed in accordance with the DCI Data and Safety Monitoring Plan. A full copy of the protocol is available on ClinicalTrials.gov.

### **Tissue handling**

Following surgery, samples were received in the surgical pathology laboratory and examined by the diagnostic staff. Frozen sections containing areas suspicious for tumor were examined by a neuropathologist. Once the diagnosis of tumor was established, tissue in excess of that required for an adequate and accurate diagnosis were collected and processed by members of the technical staff of the Duke Brain Tumor Biorepository (BTBR), a College of American Pathologists certified biorepository. Tissues were snap-frozen in liquid nitrogen either plain or embedded into Optimal Cutting Temperature (OCT) compound. If tissue samples were excessively bloody, they were rinsed with saline prior to freezing. Time as well as sample dimensions and weights were recorded at the point of freezing. At the time of surgery, whole blood was collected in tubes containing Ethylenediaminetetraacetic acid (EDTA) and placed on dry ice for transfer to storage. After freezing, samples were stored in liquid nitrogen and transferred to -80 °C prior to proteomic analysis. Sample collection details were maintained in the BTBR's Nautilus laboratory information management system (LIS), with clinical details maintained in REDCAP. After samples were checked into the BTBR LIS, they were then distributed to research teams for downstream analysis.

## **Immunohistochemistry & Immunofluorescence**

IHC and IF sectioning, staining, and imaging were performed at an external vendor (HistoWiz Inc). Staining was performed via a Leica bond automated staining platform, Akoya imager, and a proprietary processing, embedding, and grossing workflow. IHC stains were performed for CD45<sup>+</sup> (1:100, Abcam #ab40763) and CD8<sup>+</sup> (1:200, Leica #NCL-L-CD8-4B11). Triplex IF co-stained for Wheat Germ Agglutinin (WGA, 1:100, Invitrogen #W11261), MHC-I (1:3000, Cell Signaling #88274) and Glial Fibrillary Acidic Protein (GFAP, 1:6000, Novus #NB300-141) with 4',6-diamidino-2-phenylindole (DAPI) counterstain.

## **Mass Spectroscopy**

For targeted assay development, 30 µg of neat evolocumab, or 30 or 100 pmol evolocumab in 20 µL of pooled human plasma (Golden West Diagnostics) were processed as previously described<sup>22</sup>. A complete description of targeted assay development is included within the supplementary materials.

For targeted quantification of evolocumab in whole blood, 20 µL of EDTA-blood was spiked with 2 pmol of JPT SpikeTides TQL peptides with the sequences ASGYTLTSYGISWVR, GTMTTDPSTSTAYMELR and GYGMDVWVGQTTVTVSSASTK (and 10 pmol of evolocumab in positive control samples) followed by deoxycholate-assisted trypsin digestion and microflow LC-MS/MS with solvent divert as described previously<sup>22</sup>. Briefly, deoxycholate-assisted trypsin digestion was used above except that 500 µg of TPCK-trypsin was used and reactions were quenched with 2% TFA. An external calibration curve was generated using evolocumab in whole blood from a control subject, and quantification to standard curve was performed using Skyline. Blood levels (normalized to volume) were further normalized to microgram protein (fmol/µg) based on an estimated protein concentration in blood of 250 µg/µL.

Fresh frozen tissue either directly frozen or embedded in OCT were analyzed using targeted and non-targeted proteomics. A full description of methods used for targeted and non-targeted proteomics is also provided within the supplementary materials.

## **Spatial RNA sequencing**

Formalin-fixed paraffin-embedded (FFPE) tissues were processed for spatial in situ sequencing transcriptomic profiling. 5µm FFPE tissue sections were placed on a 10x Genomics (Pleasanton, CA) Xenium slide and incubated at 42C for 3 hours, prior to being deparaffinized and decrosslinked via immersion in xylene and ethanol, and hydrated in water to remove residual ethanol. Once hydrated, tissues slides were decrosslinked. Tissue slides were then inserted into 10x Genomics Xenium slide cassettes.

Decrosslinking buffer was added to the well created by the cassette and incubated. After incubation, buffer was removed, and the sample was washed. Tissue was then processed through Hybridization, Ligation & Amplification protocols. These protocols are described fully within the supplementary materials.

For analysis of each Xenium sample, centroid (location), segmentation (cell boundaries), and the counts matrix data were extracted. Cells were filtered to have more than five features and more than ten counts. These were normalized and run through the Banksy functions (Prabhakar lab<sup>42</sup>) with a lambda of 0.2 for the Banksy matrix computation and a resolution of 1.0 for maximum clusters. Gene expression was calculated as an average of counts for each gene in each cluster and then normalized by dividing each cluster's average gene expression by the maximum average cluster expression for that gene. Hierarchical cluster heatmaps to aid with

annotation were generated using clustergrammer (Maayan lab<sup>43</sup>), following normalization of raw gene counts using the logCPM method, before transformation using the Z-score method. Most probable annotations were then mapped back onto the clusters and used to color code visuals by cell type. UMAPs were made for each grade (IV and low), and spatial plots were generated for each sample. These create an informative representative of the original FFPE slide. Niches were made by facet-wrapping these spatial plots by cell type, allowing direct visualization of each layer (cell type). Differential expression analyses highlighted immune-tumor dynamics in pro-inflammatory and immunosuppressive pathways.

### **Statistical analysis plan**

Up to 10 patients were to be enrolled in the treatment arm of this study, while up to 20 patients served as controls. The sample size selected was chosen for practical considerations in the setting of a phase 0 study, to allow descriptive analysis of the changes of the biologic endpoints in the evolocumab treated (cases) and untreated patients (controls). For analysis of the level of evolocumab within the resected or biopsied tumor, this was to be compared with resected or biopsied control patients who were not treated with evolocumab via either a Wilcoxon rank sum test or a two-sample t-test, with adjustment for multiple comparisons. Assessment of the relationship between serum and intratumoral levels of drug were to be performed by using a scatterplot to graphically show the relationship between these two measures with spearman's rank correlation used to assess association. Within this study, experimental results are presented as mean  $\pm$  SD unless otherwise specified. Statistical tests for all studies were completed using GraphPad v.8.4.3 (Prism). Asterisks were appended to graphs to represent the significance level of any difference (\* $p \leq 0.05$ , \*\* $p \leq 0.01$ , \*\*\* $p \leq 0.001$ , \*\*\*\* $p \leq 0.0001$ ,  $p > 0.05$  not significant). Comparisons between groups were performed using a two-tailed Mann-Whitney U test. Correlation analyses were performed using the Pearson correlation coefficient.

## References and Notes:

- 1 Cornel, A. M., Mimpfen, I. L. & Nierkens, S. MHC class I downregulation in cancer: underlying mechanisms and potential targets for cancer immunotherapy. *Cancers* **12**, 1760 (2020).
- 2 Morrison, B. J., Steel, J. C. & Morris, J. C. Reduction of MHC-I expression limits T-lymphocyte-mediated killing of Cancer-initiating cells. *BMC cancer* **18**, 1-10 (2018).
- 3 Mina, M. *et al.* Tumor-infiltrating T lymphocytes improve clinical outcome of therapy-resistant neuroblastoma. *OncImmunology* **4**, e1019981 (2015). <https://doi.org/10.1080/2162402X.2015.1019981>
- 4 Lerner, E. C. *et al.* CD8+ T cells maintain killing of MHC-I-negative tumor cells through the NKG2D–NKG2DL axis. *Nature Cancer* **4**, 1258-1272 (2023). <https://doi.org/10.1038/s43018-023-00600-4>
- 5 Garrido, F., Aptsiauri, N., Doorduijn, E. M., Lora, A. M. G. & Van Hall, T. The urgent need to recover MHC class I in cancers for effective immunotherapy. *Current opinion in immunology* **39**, 44-51 (2016).
- 6 Liu, X. *et al.* Inhibition of PCSK9 potentiates immune checkpoint therapy for cancer. *Nature* **588**, 693-698 (2020). <https://doi.org/10.1038/s41586-020-2911-7>
- 7 Poirier, S. *et al.* The proprotein convertase PCSK9 induces the degradation of low density lipoprotein receptor (LDLR) and its closest family members VLDLR and ApoER2. *J Biol Chem* **283**, 2363-2372 (2008). <https://doi.org/10.1074/jbc.M708098200>
- 8 Demers, A. *et al.* PCSK9 Induces CD36 Degradation and Affects Long-Chain Fatty Acid Uptake and Triglyceride Metabolism in Adipocytes and in Mouse Liver. *Arterioscler Thromb Vasc Biol* **35**, 2517-2525 (2015). <https://doi.org/10.1161/atvbaha.115.306032>
- 9 Uhlén, M. *et al.* Tissue-based map of the human proteome. *Science* **347**, 1260419 (2015). <https://doi.org/doi:10.1126/science.1260419>
- 10 Singh, K. *et al.* Designing Clinical Trials for Combination Immunotherapy: A Framework for Glioblastoma. *Clinical cancer research : an official journal of the American Association for Cancer Research* **28**, 585-593 (2022). <https://doi.org/10.1158/1078-0432.Ccr-21-2681>
- 11 Sabatine, M. S. *et al.* Efficacy and Safety of Evolocumab in Reducing Lipids and Cardiovascular Events. *New England Journal of Medicine* **372**, 1500-1509 (2015). <https://doi.org/10.1056/NEJMoa1500858>
- 12 Sabatine, M. S. PCSK9 inhibitors: clinical evidence and implementation. *Nature Reviews Cardiology* **16**, 155-165 (2019). <https://doi.org/10.1038/s41569-018-0107-8>
- 13 Schwartz, G. G. *et al.* Alirocumab and Cardiovascular Outcomes after Acute Coronary Syndrome. *New England Journal of Medicine* **379**, 2097-2107 (2018). <https://doi.org/doi:10.1056/NEJMoa1801174>
- 14 Seidah, N. G. & Prat, A. The biology and therapeutic targeting of the proprotein convertases. *Nat Rev Drug Discov* **11**, 367-383 (2012). <https://doi.org/10.1038/nrd3699>
- 15 Fitzgerald, K. *et al.* A Highly Durable RNAi Therapeutic Inhibitor of PCSK9. *The New England journal of medicine* **376**, 41-51 (2017). <https://doi.org/10.1056/NEJMoa1609243>
- 16 Gibbs, J. P. *et al.* Impact of Target-Mediated Elimination on the Dose and Regimen of Evolocumab, a Human Monoclonal Antibody Against Proprotein Convertase Subtilisin/Kexin Type 9 (PCSK9). *The Journal of Clinical Pharmacology* **57**, 616-626 (2017). <https://doi.org/https://doi.org/10.1002/jcph.840>
- 17 Pardridge, W. M. Blood-Brain Barrier and Delivery of Protein and Gene Therapeutics to Brain. *Frontiers in Aging Neuroscience* **11** (2020). <https://doi.org/10.3389/fnagi.2019.00373>
- 18 Sarkaria, J. N. *et al.* Is the blood-brain barrier really disrupted in all glioblastomas? A critical assessment of existing clinical data. *Neuro-oncology* **20**, 184-191 (2018). <https://doi.org/10.1093/neuonc/nox175>
- 19 Portnow, J. *et al.* Systemic Anti-PD-1 Immunotherapy Results in PD-1 Blockade on T Cells in the Cerebrospinal Fluid. *JAMA oncology* **6**, 1947-1951 (2020). <https://doi.org/10.1001/jamaoncol.2020.4508>
- 20 Schulz, K. F., Altman, D. G. & Moher, D. CONSORT 2010 statement: updated guidelines for reporting parallel group randomised trials. *Bmj* **340**, c332 (2010). <https://doi.org/10.1136/bmj.c332>
- 21 Schaeffer, M. *et al.* The neXtProt peptide uniqueness checker: a tool for the proteomics community. *Bioinformatics* **33**, 3471-3472 (2017). <https://doi.org/10.1093/bioinformatics/btx318>
- 22 Schaller, T. H. *et al.* Pharmacokinetic Analysis of a Novel Human EGFRvIII:CD3 Bispecific Antibody in Plasma and Whole Blood Using a High-Resolution Targeted Mass Spectrometry Approach. *J Proteome Res* **18**, 3032-3041 (2019). <https://doi.org/10.1021/acs.jproteome.9b00145>
- 23 Jung, T. Y. *et al.* Immunological characterization of glioblastoma cells for immunotherapy. *Anticancer research* **33**, 2525-2533 (2013).
- 24 Mahley, R. W. Central Nervous System Lipoproteins. *Arteriosclerosis, Thrombosis, and Vascular Biology* **36**, 1305-1315 (2016). <https://doi.org/doi:10.1161/ATVBAHA.116.307023>

- 25 Armocida, D., Frati, A., Salvati, M., Santoro, A. & Pesce, A. Is Ki-67 index overexpression in IDH wild type glioblastoma a  
predictor of shorter Progression Free survival? A clinical and Molecular analytic investigation. *Clinical neurology and*  
*neurosurgery* **198**, 106126 (2020). <https://doi.org/https://doi.org/10.1016/j.clineuro.2020.106126>
- 26 Reardon, D. A. *et al.* Effect of Nivolumab vs Bevacizumab in Patients With Recurrent Glioblastoma: The CheckMate 143  
Phase 3 Randomized Clinical Trial. *JAMA Oncology* **6**, 1003-1010 (2020). <https://doi.org/10.1001/jamaoncol.2020.1024>
- 27 Geraghty, D. E., Koller, B. H., Hansen, J. A. & Orr, H. T. The HLA class I gene family includes at least six genes and twelve  
pseudogenes and gene fragments. *J Immunol* **149**, 1934-1946 (1992).
- 28 Paganini, J. *et al.* HLA-B worldwide genetic diversity: New HLA-B alleles and haplotype structure description. *Mol Immunol*  
**112**, 40-50 (2019). <https://doi.org/10.1016/j.molimm.2019.04.017>
- 29 Jordier, F. *et al.* HLA-H: Transcriptional Activity and HLA-E Mobilization. *Front Immunol* **10**, 2986 (2019).  
<https://doi.org/10.3389/fimmu.2019.02986>
- 30 Maddison, K. *et al.* Low tumour-infiltrating lymphocyte density in primary and recurrent glioblastoma. *Oncotarget* **12**, 2177-  
2187 (2021). <https://doi.org/10.18632/oncotarget.28069>
- 31 Robinson, M. H. *et al.* Subtype and grade-dependent spatial heterogeneity of T-cell infiltration in pediatric glioma. *Journal*  
*for ImmunoTherapy of Cancer* **8**, e001066 (2020). <https://doi.org/10.1136/jitc-2020-001066>
- 32 Miao, G. *et al.* From degenerative disease to malignant tumors: Insight to the function of ApoE. *Biomedicine &*  
*Pharmacotherapy* **158**, 114127 (2023). <https://doi.org/https://doi.org/10.1016/j.biopha.2022.114127>
- 33 Lanfranco, M. F., Sepulveda, J., Kopetsky, G. & Rebeck, G. W. Expression and secretion of apoE isoforms in astrocytes and  
microglia during inflammation. *Glia* **69**, 1478-1493 (2021).
- 34 Zhang, H., Wu, L.-M. & Wu, J. Cross-talk between apolipoprotein E and cytokines. *Mediators of inflammation* **2011** (2011).
- 35 Baitsch, D. *et al.* Apolipoprotein E induces antiinflammatory phenotype in macrophages. *Arteriosclerosis, thrombosis, and*  
*vascular biology* **31**, 1160-1168 (2011).
- 36 Khan, F. *et al.* Macrophages and microglia in glioblastoma: heterogeneity, plasticity, and therapy. *The Journal of clinical*  
*investigation* **133** (2023). <https://doi.org/10.1172/JCI163446>
- 37 Liao, F. *et al.* Anti-ApoE antibody given after plaque onset decreases A $\beta$  accumulation and improves brain function in a  
mouse model of A $\beta$  amyloidosis. *Journal of Neuroscience* **34**, 7281-7292 (2014).
- 38 Kaji, S. *et al.* Apolipoprotein E aggregation in microglia initiates Alzheimer's disease pathology by seeding  
&#x3b2;-amyloidosis. *Immunity* **57**, 2651-2668.e2612 (2024). <https://doi.org/10.1016/j.immuni.2024.09.014>
- 39 Huang, Y. *et al.* Cavitation Feedback Control of Focused Ultrasound Blood-Brain Barrier Opening for Drug Delivery in  
Patients with Parkinson's Disease. *Pharmaceutics* **14** (2022). <https://doi.org/10.3390/pharmaceutics14122607>
- 40 Chen, P. Y. *et al.* Focused ultrasound-induced blood-brain barrier opening to enhance interleukin-12 delivery for brain tumor  
immunotherapy: a preclinical feasibility study. *J Transl Med* **13**, 93 (2015). <https://doi.org/10.1186/s12967-015-0451-y>
- 41 Kalita, T., Dezfouli, S. A., Pandey, L. M. & Uludag, H. siRNA Functionalized Lipid Nanoparticles (LNPs) in Management of  
Diseases. *Pharmaceutics* **14** (2022). <https://doi.org/10.3390/pharmaceutics14112520>
- 42 Singhal, V. *et al.* BANKSY unifies cell typing and tissue domain segmentation for scalable spatial omics data analysis.  
*Nature genetics* **56**, 431-441 (2024). <https://doi.org/10.1038/s41588-024-01664-3>
- 43 Fernandez, N. F. *et al.* Clustergrammer, a web-based heatmap visualization and analysis tool for high-dimensional biological  
data. *Scientific Data* **4**, 170151 (2017). <https://doi.org/10.1038/sdata.2017.151>
- 44 Pino, L. K. *et al.* The Skyline ecosystem: Informatics for quantitative mass spectrometry proteomics. *Mass Spectrom Rev* **39**,  
229-244 (2020). <https://doi.org/10.1002/mas.21540>
- 45 Dorfer, V. *et al.* MS Amanda, a universal identification algorithm optimized for high accuracy tandem mass spectra. *J*  
*Proteome Res* **13**, 3679-3684 (2014). <https://doi.org/10.1021/pr500202e>
- 46 Käll, L., Canterbury, J. D., Weston, J., Noble, W. S. & MacCoss, M. J. Semi-supervised learning for peptide identification  
from shotgun proteomics datasets. *Nat Methods* **4**, 923-925 (2007). <https://doi.org/10.1038/nmeth1113>
- 47 Zahn-Zabal, M. *et al.* The neXtProt knowledgebase in 2020: data, tools and usability improvements. *Nucleic Acids Res* **48**,  
D328-d334 (2020). <https://doi.org/10.1093/nar/gkz995>
- 48 Guzman, U. H. *et al.* Ultra-fast label-free quantification and comprehensive proteome coverage with narrow-window data-  
independent acquisition. *Nat Biotechnol* (2024). <https://doi.org/10.1038/s41587-023-02099-7>
- 49 Heil, L. R. *et al.* Evaluating the Performance of the Astral Mass Analyzer for Quantitative Proteomics Using Data-  
Independent Acquisition. *J Proteome Res* **22**, 3290-3300 (2023). <https://doi.org/10.1021/acs.jproteome.3c00357>
- 50 Demichev, V., Messner, C. B., Vernardis, S. I., Lilley, K. S. & Ralser, M. DIA-NN: neural networks and interference  
correction enable deep proteome coverage in high throughput. *Nat Methods* **17**, 41-44 (2020).  
<https://doi.org/10.1038/s41592-019-0638-x>

# Acknowledgements:

## General

We are grateful to all patients and their caregivers who enrolled in this study. We are also grateful to the Knox Martin Foundation and the Langford Cregger Foundation for their philanthropic support. We are also grateful to the team at the Duke Brain Tumor Biorepository for their assistance and co-ordination in tissue management and acquisition. We would also like to acknowledge the assistance of the Molecular Genomics Core at the Duke Molecular Physiology Institute, Duke University School of Medicine, for the generation of data for the manuscript.

## Funding

Knox Martin Foundation, Philanthropic Grant (MK)

Langford Cregger Foundation, Philanthropic Grant (MK)

## Author contributions

Conceptualization: KS, MK

Methodology: KS, MWF, MJV, MK

Investigation: KS, MWF, MJV, AMC, ELT, KMH, COR, EEB, DMA, AD, HSF, MOJ, AF, SK, JHS, APP, SGG, CYL

Pathology: GYL, REM

Neuroradiology: EC

Spatial RNA sequencing, AMC, KS

Writing – original draft: KS, MWF, PEF, MK

Writing – review & editing: KS, MWF, MJV, AMC, ELT, KMH, COR, EEB, DMA, AD, HSF, MOJ, AF, SK, JHS, APP, SGG, CYL, PEF, MK

Statistical analysis: KS, EDB, JEH

Supervision: PEF, MK

## Competing Interests

MWF, MJV, AMC, KMH, COR, EEB, KEB, ELT, DMA, AD, HSF, MOJ, AF, SK, EDB, JEH, REM, EC, GAG, SGG, CYL declare that they have no competing interests. KS reports grants paid to his institution and research contracts from Adaptin Bio, which has licensed intellectual property from Duke related to the use of Brain Bi-specific T cell Engagers (BRiTE) and combination autologous lymphocyte therapy. JHS reports an equity interest in Istari Oncology, which has licensed intellectual property from Duke related to the use of poliovirus and D2C7 in the treatment of glioblastoma. JHS is an inventor on patents related to Brain Bi-specific T cell Engagers (BRiTE), PEP-CMV DC vaccine with tetanus, as well as poliovirus vaccine and D2C7 in the treatment of glioblastoma. GYL reports consulting fees from Servier Pharmaceuticals. GYL is a consultant for and has equity in SNPsnipe, Inc. APP is a consultant for Sygnomics, Syapse, and Servier Pharmaceuticals, and has an equity in Sygnomics. PEF reports support as an Akash fellow of the CRI Lloyd J. Old STAR award program and has received consulting fees and grant funding from Monteris Medical outside the submitted work. MK reports grants or contracts from BMS, AbbVie, BioNTech, CNS Pharmaceuticals, Daiichi Sankyo Inc., Immorna Therapeutics, Immvira Therapeutics, JAX lab for genomic research, and Personalis, Inc.; received consulting fees from

AnHeart Therapeutics, Berg Pharma, George Clinical, Manarini Stemline, and Servier; received honoraria from GSK; and is on a data safety monitoring board for BPG Bio.

### **Data and materials availability**

Targeted proteomic data have been deposited to the ProteomeXchange Consortium (PXD053215) via the Panorama Public repository (<https://panoramaweb.org/ccb1LM.url>). While the manuscript is under review, the data can be accessed via reviewer credentials email: [panorama+reviewer272@proteinms.net](mailto:panorama+reviewer272@proteinms.net) and password: “3aF%#D9KuT&yA”. All demographic, AE, flow cytometry and ISS/IHC/IF data are available in the main text.

## **Supplementary Materials:**

### **List:**

**Fig. S1.** Mechanism of PCSK9i for increasing surface MHC-I

**Fig. S2.** Trial study schema

**Fig. S3.** Clustering heatmap for grade IV gliomas

**Fig. S4.** Clustering heatmap for grade II/III gliomas

**Fig. S5.** H&E staining for grade IV tumor with high evolocumab uptake (ID: 1007) used for paired ISS/IHC/IF

**Fig. S6.** Paired ISS/IHC/IF for grade II tumor with low evolocumab uptake (ID: 1008)

**Fig. S7.** H&E staining for grade II tumor with low evolocumab uptake (ID: 1008)

**Table. S1.** Full inclusion & exclusion criteria for study

No supplementary materials specific references are included

## Main Figures:

**Fig. 1. Relative plasma concentrations of PCSK9 in blood from patients with different cancer types**

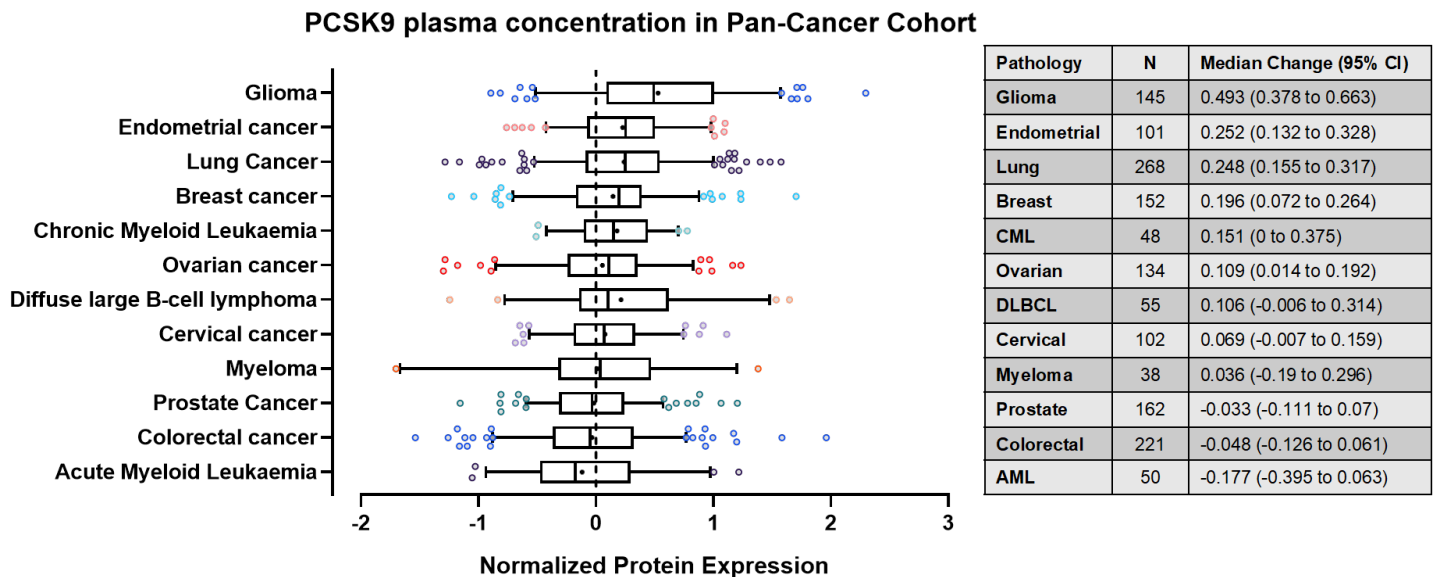
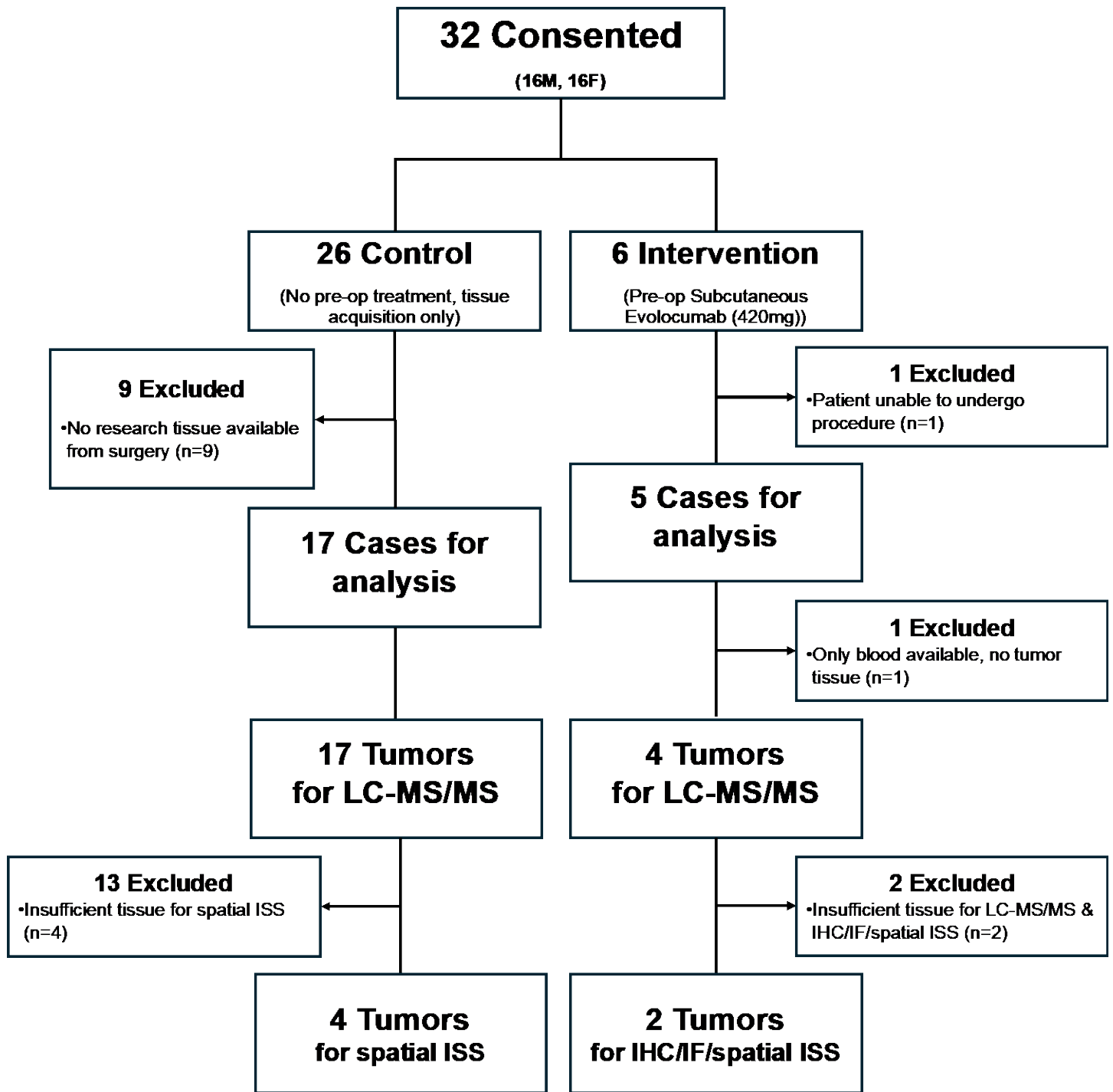


**Fig. 1. Relative plasma concentrations of PCSK9 in blood from patients with different cancer types**

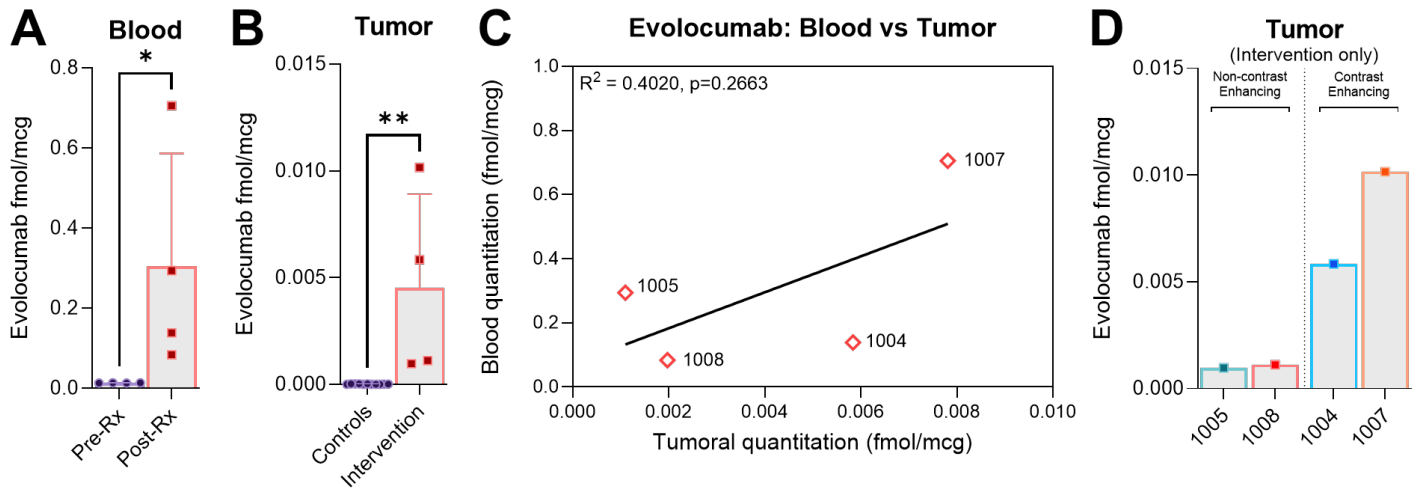
Box and whisker representations of circulating concentrations of PCSK9 protein in plasma across multiple cancer types. Circulating plasma PCSK9 protein levels are the most upregulated in glioma compared to the average concentration from samples across multiple. Assessed by proximity extension assay (PEA). Whiskers represent 5-95% range with outliers shown. Mean shown as +. Data from proteinatlas.org (<https://www.proteinatlas.org/ENSG00000169174-PCSK9/disease>).

Fig. 2. CONSORT flow diagram of enrolled participants



\*Tissue only collected for research purposes if excess available beyond that required for clinical pathology.  
 LC-MS/MS: Liquid chromatography coupled to tandem mass spectrometry IHC: Immunohistochemistry, IF: Immunofluorescence, ISS: *In situ sequencing*

**Fig. 3. Peripherally administered evolocumab is detected in intracranial tumors, with enhanced titers in contrast-enhancing disease**



**Fig. 3. Peripherally administered evolocumab is detected in intracranial tumors, with enhanced titers in contrast-enhancing disease**

(A) Evolocumab levels in peripheral blood (1004: 0.1383 fmol/mcg, 1005: 0.2940 fmol/mcg, 1007: 0.7052 fmol/mcg, 1008: 0.0836 fmol/mcg). No evolocumab was detected in pre-treatment blood samples ( $p=0.0286^*$ ). Detection via most specific evolocumab detection peptide (GTMTTDPSTSTAYMELR) shown in analysis. Detection is normalized to stable internally labelled (SIL) peptide controls. Comparison via two-tailed Mann Whitney U test.

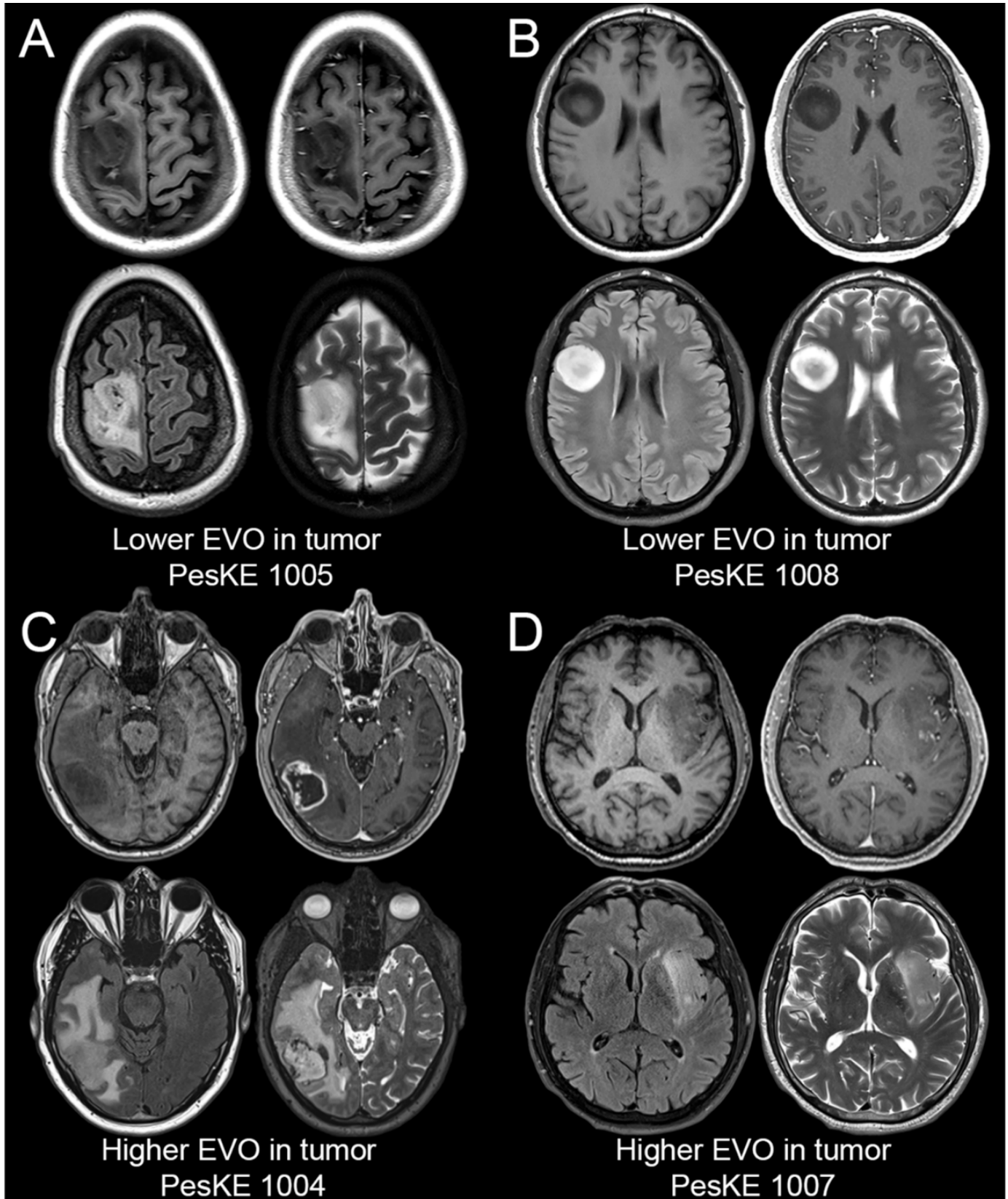
(B) Evolocumab levels in tumor compared to controls. Drug was detected in all intervention cases post subcutaneous administration, with negligible background signal detected in non-treatment controls ( $p=0.0015^{**}$ , two two-tailed Mann Whitney U test).

(C) Scatterplot showing a positive but non-significant relationship between evolocumab titers in blood and evolocumab titers in tumor ( $R^2 = 0.4020$ ,  $p=0.2663$ , Pearson's Correlation Coefficient). The average tumor: blood ratio of evolocumab was 0.0222 ( $SD\pm 0.0190$ ). Average across individual detection peptides shown (sequences that are not part of the human proteome but identify drug: ASGYTLTSYGISWVR, GTMTTDPSTSTAYMELR and GYGMDVWVGQTTTVSSASTK). Detection is normalized to stable internally labelled (SIL) peptide controls.

(D) Evolocumab detection was higher in cases 1004 and 1007 (0.005838 fmol/mcg and 0.01016 fmol/mcg respectively), whereas detection was lower in cases 1005 and 1008 (0.000964 fmol/mcg and 0.001118 fmol/mcg respectively). The greatest uptake ratio was observed in the case with the highest degree of contrast-enhancement on MRI (ID: 1004, tumor: blood ratio of 0.0547, MRI shown in Fig. 4C).

Data presented as mean  $\pm$  SD unless otherwise specified.

**Fig. 4. MRI sequences of tumors with lower and higher evolocumab (EVO) uptake**



*Representative pre-operative brain MRI images of intervention tumors. For each panel A-D, axial images through the tumor are shown from four standard anatomic image series (clockwise from left: T1-weighted pre-contrast, T1-weighted post-contrast, T2-weighted, and T2-weighted FLAIR).*

**Fig. 4. MRI sequences of tumors with lower and higher evolocumab (EVO) uptake**

(A & B) Evaluation of pre-operative MR imaging from cases 1005 (grade III Oligodendroglioma) and 1008 (grade II Astrocytoma) with lower evolocumab uptake reveals non-contrast-enhancing lesions on T1 post sequences (quadrant top-right).

(C & D) Conversely, evaluation of pre-operative MR imaging from cases 1004 and 1007 (both grade IV glioblastomas) with higher evolocumab uptake reveals evidence of contrast-enhancement on T1 post sequences (quadrant top-right).

Representative pre-operative brain MRI images of analyzed tumors. For each panel A-D, axial images through the tumor are shown from four standard anatomic image series (clockwise from left: T1-weighted pre-contrast, T1-weighted post-contrast, T2-weighted, and T2-weighted FLAIR).

**Fig. 5. Higher evolocumab uptake in tumor is associated with increased MHC-I and decreased Apolipoprotein E quantities within the tumor proteome**

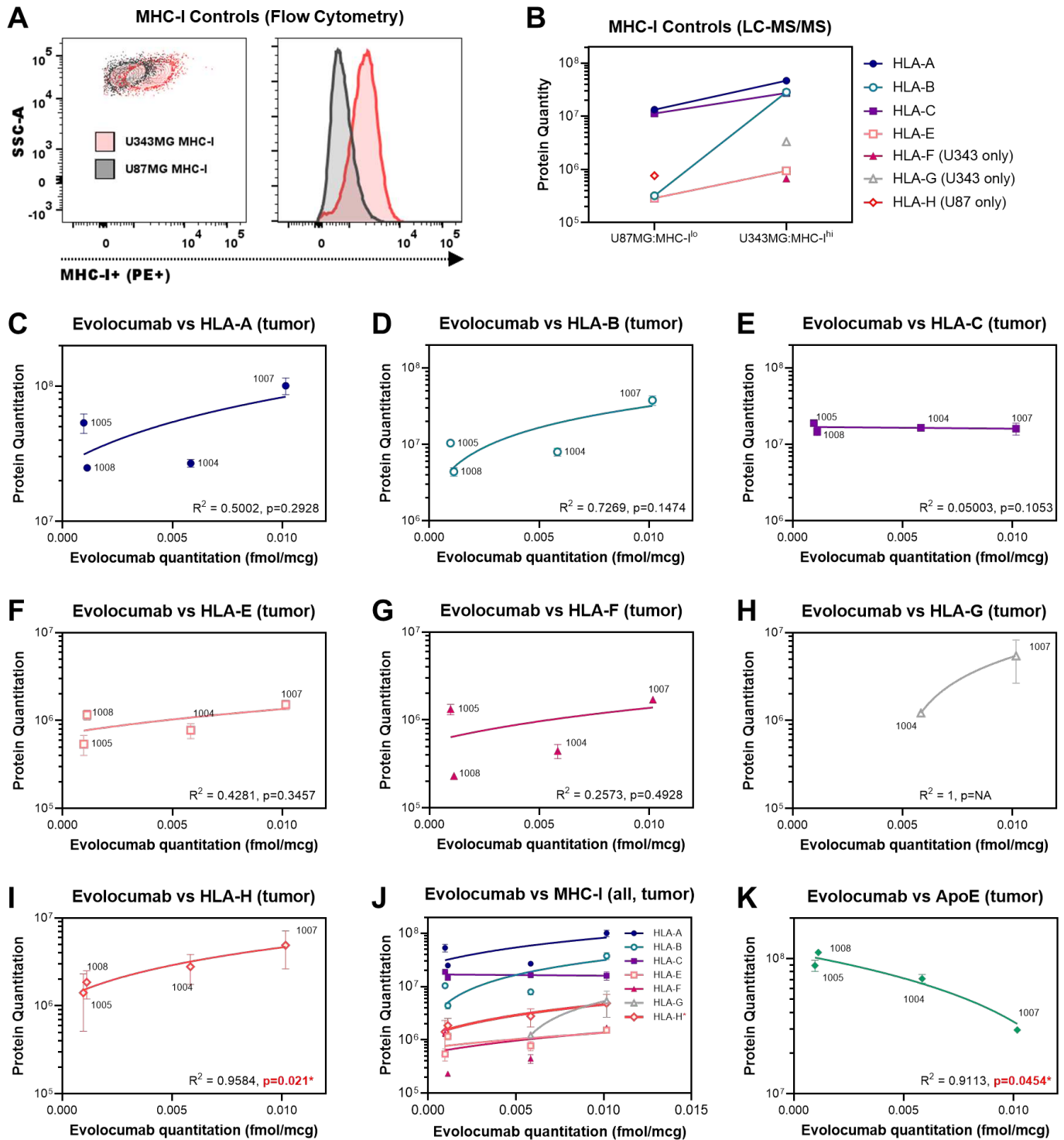


**Fig. 5. Higher evolocumab uptake in tumor is associated with increased MHC-I and decreased Apolipoprotein E quantities within the tumor proteome**

(A) Flow cytometric analysis of immortalized human glioma lines thought to express higher (U343MG, red) or lower (U87MG, black) levels of MHC-I. Staining for HLA-ABC confirms that U343MG is MHC-I<sup>Hi</sup>, while U87MG is MHC-I<sup>Lo</sup>.

(B) Non-targeted LC/MS-MS quantitation of the tumor proteome reveals that U343MG has higher overall protein quantities of HLA-A, -B, -C and -E, compared to U87MG (HLA-A: U343MG vs U87MG  $4.67 \times 10^7$  vs  $1.33 \times 10^7$ , HLA-B:  $2.85 \times 10^7$  vs  $3.22 \times 10^5$ , HLA-C:  $2.75 \times 10^7$  vs  $1.13 \times 10^7$ , HLA-E:  $9.43 \times 10^5$  vs  $2.91 \times 10^5$ ). Non-targeted proteome analysis yielded incomplete data for HLA-F, HLA-G and HLA-H (data included). These findings were in keeping with our flow cytometric analysis in (A) and provides validation for our detection method for MHC-I subtypes in tumors.

(C) A positive but non-significant correlation was observed between intratumoral evolocumab and HLA-A protein levels ( $R^2=0.5002$ ,  $p=0.2928$ ,  $n=4$ ).

(D) Similar trends were observed between intratumoral evolocumab and HLA-B protein levels ( $R^2=0.7269$ ,  $p=0.1474$ ,  $n=4$ ).

(E) No change in HLA-C levels were observed in response to intratumoral evolocumab ( $R^2=0.05003$ ,  $p=0.1053$ ,  $n=4$ ).

(F-H) Positive but non-significant correlative trends were also observed for HLA-E ( $R^2=0.4281$ ,  $p=0.3457$ ,  $n=4$ ), HLA-F ( $R^2=0.2573$ ,  $p=0.4928$ ,  $n=4$ ) and HLA-G ( $R^2=1$ ,  $p=NA$ ,  $n=2$ , incomplete non-targeted proteome analysis yielded no data for ID: 1005 or ID: 1008 via LC-MS/MS).

(I) A significant positive correlation was observed between intratumoral evolocumab and HLA-H protein levels ( $R^2=0.9584$ ,  $p=0.021^*$ ,  $n=4$ ).

(J) Trends across all MHC-I subtypes in relation to intratumoral evolocumab shown.

(K) Evaluation of Apolipoprotein E levels across intervention samples found a significant negative trend between ApoE and intratumoral evolocumab ( $R^2=0.9113$ ,  $p=0.0454^*$ ).

Data presented as mean  $\pm$  SD unless otherwise specified. Correlation analyses were performed using Pearson's Correlation Coefficient (PCC). Trendlines shown reflect simple linear regression.

**Fig. 6. Increased cytotoxic CD8<sup>+</sup> T cell infiltration and MHC-I cell surface expression is observed near proliferating tumor cells in tissue with higher evolocumab titers**

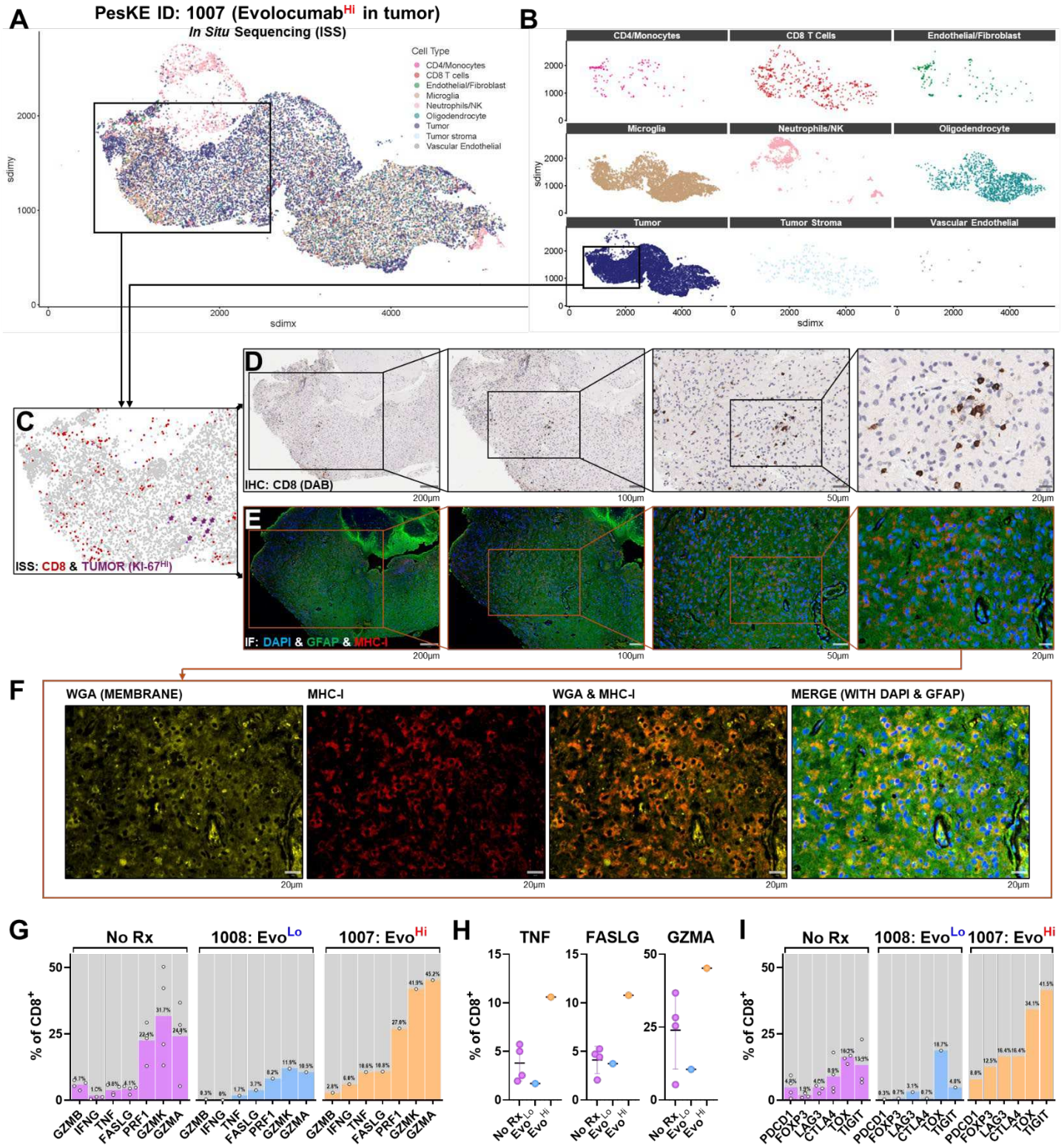


**Fig. 6. Increased cytotoxic CD8<sup>+</sup> T cell infiltration and MHC-I cell surface expression is observed near proliferating tumor cells in tissue with higher evolocumab titers**

(A & B) Paired in situ RNA sequencing (ISS) via Xenium platform and individual niches shown. Boxed region indicates areas of tumor as assessed by H&E and transcriptomic analysis.

(C) Area of interest shown with Ki-67<sup>Hi</sup> (i.e., proliferating) tumor highlighted in purple (with arrows) and CD8<sup>+</sup> T cells highlighted in red, as identified via *in situ* sequencing. Overall tumor is shown in background (gray).

(D-F) Paired Immunohistochemistry (IHC) and Immunofluorescence (IF) from tissue samples from a case with high evolocumab uptake adjacent to region of Ki-67<sup>Hi</sup> tumor (ID: 1007, grade IV glioblastoma). High levels of parenchymal CD8<sup>+</sup> infiltration within the parenchyma adjacent to proliferating tumor cells are observed on IHC staining. IF staining of GFAP (green), DAPI (nuclei, blue) and MHC-I (red) shows increased MHC-I expression in regions which co-localized with areas of CD8<sup>+</sup> infiltrate. Staining with WGA (yellow) demonstrates MHC-I co-localized with cell membranes.

(G) Transcriptomic comparison of the fraction of CD8<sup>+</sup> cells expressing markers of cytotoxic activity (*GZMB*, *IFNG*, *TNF*, *FASLG*, *PRFI*, *GZMK*, *GZMA*) between untreated controls, and tumor tissue with low (ID: 1008) or high (ID: 1007) evolocumab uptake

(H) Evaluation of most differentially expressed markers reveals that *TNF*, *FASLG* and *GZMA* were most increased in tumor tissue with high (ID: 1007) evolocumab uptake (evolocumab high vs non-treated % CD8<sup>+</sup>: *TNF* 2.78x, *FASLG* 2.62x, *GZMA* 1.89x)

(I) Transcriptomic comparison of the fraction of CD8<sup>+</sup> cells expressing markers of T cell exhaustion (*PDCD1*, *FOXP3*, *LAG3*, *CTLA4*, *TOX*, *TIGIT*) between untreated controls, and tumor tissue with low (ID: 1008) or high (ID: 1007) evolocumab uptake.

Data presented as mean ± SD unless otherwise specified.

## Supplementary Materials (separate)

- Supplementary Methods
- **Fig. S1.** Trial study schema
- **Fig. S2.** Clustering heatmap for grade IV gliomas
- **Fig. S3.** Clustering heatmap for grade II/III gliomas
- **Fig. S4.** H&E staining for grade IV tumor with high evolocumab uptake (ID: 1007) used for paired ISS/IHC/IF
- **Fig. S5.** Paired ISS/IHC/IF for grade II tumor with low evolocumab uptake (ID: 1008)
- **Fig. S6.** H&E staining for grade II tumor with low evolocumab uptake (ID: 1008)
- **Table S1.** Full inclusion & exclusion criteria for study
- **Table S2.** Demographics of consented participants
- **Table S3.** Toxicity summary of all Adverse Events among participants treated with evolocumab
- **Table S4.** Toxicity summary of Adverse Events among participants possibly, probably, or definitely related to evolocumab

## Supplementary Methods

### Mass Spectroscopy

For targeted assay development, samples were diluted to 200  $\mu$ L with 5% deoxycholate and 10 mM dithiothreitol (DTT) followed by heating at 80  $^{\circ}$ C for 20 min using a Thermomixer (Eppendorf). After cooling, alkylation was performed with 25 mM iodoacetamide in the dark for 30 min followed by the addition of 100  $\mu$ g of TPCK-trypsin (Worthington) and incubation at 37  $^{\circ}$ C for 2 h. After quenching with 1.5% trifluoroacetic acid and filtering, digests were analyzed by a 20 min microflow LC-MS/MS using a Waters ACQUITY UPLC (1 x 100 mm or 1 x 150 mm ACQUITY Premier CSH column; direct injection; 100  $\mu$ L/min flow rate; 3-28% MeCN-0.1% formic acid) interfaced to a Thermo Exploris 480. Neat Evo was analyzed by data-dependent acquisition, and database searching was performed with Skyline<sup>44</sup> using the MS Amanda search engine with Percolator post-search validation<sup>45,46</sup>. Peptide uniqueness was predicted using NCBI BLASTp and Nextprot peptide uniqueness checker<sup>47</sup>. Candidate proteotypic peptides were analyzed in the evolocumab-spiked plasma using parallel reaction monitoring as previously described. Data were analyzed in Skyline and have been uploaded to the ProteomeXchange consortium (details in data and materials availability sub-section).

For targeted and non-targeted proteomics, tissue was rinsed free with cold phosphate-buffered saline and homogenized by sonication or bead beating in a 10:1 volume per tissue weight of 5% (w/v) sodium dodecyl sulfate in 50 mM triethylammonium bicarbonate. Based on detergent-compatible Bradford assay, 20  $\mu$ g of each sample was reduced and alkylated and digested with 2 or 10  $\mu$ g Sequencing Grade Modified Trypsin (Promega) using an S-trap micro device (Protifi) and 47  $^{\circ}$ C for 1 h. 200 fmol of SpikeTides TQL peptides were added to the S-trap along with trypsin. After elution, peptides were lyophilized, reconstituted in 0.2 % formic acid, and a study pool QC (SPQC) sample was made by mixing equal amounts of all samples. Approximately 1  $\mu$ g of each sample, along with replicates of a study pool QC (SPQC), were loaded onto Evotip Pure tips. Targeted proteomic analysis used an Evosep One LC interfaced to a Thermo Exploris 480 and analyzed using a 100 sample-per-day (100SPD) LC method and PRM as described above. During method development, 100  $\mu$ g of select samples were digested with 10  $\mu$ g trypsin, and 30  $\mu$ g of digested were analyzed by microflow LC-MS/MS as with the whole blood. Data was analyzed in Skyline and normalized to stable isotope-labeled internal standard (at 10 fmol/ $\mu$ g) to derive femtomol per microgram values of evolocumab in tumor.

Non-targeted proteomics used an Evosep One LC interfaced to a Thermo Orbitrap Astral using a 60 sample-per-day (60SPD) LC method and data-independent acquisition (DIA) in the Astral analyzer<sup>48,49</sup>. MS/MS used 150 x 4 m/z windows from 380-980 m/z, and automatic gain control target of 500%, 6 ms ion transfer time and normalized collision energy of 28. Data was analyzed with DIA-NN 1.8.2 beta 27 in library-free mode<sup>50</sup>. Raw data was converted to .dia before processing. Default settings were used with trypsin specificity and up to 2 missed cleavage, and N-terminal acetylation as a variable modification, Identification and quantification used a 1% precursor and protein group false discovery rate. Data was further filtered to include protein groups with no missing data and %coefficient of variation <50 across four analyses of a QC pool.

### Spatial RNA sequencing

Xenium samples were processed by first adding a panel containing 480 custom gene padlock probes enriched in genes relevant to cell type and cell state, including glioma, neuronal and immune cells to the tissue. Each circularizable DNA probe contains two regions that hybridize to target RNA and a third region that encodes a gene-specific barcode. The two ends of the probes bind the target RNA

and are ligated to generate a circular DNA probe. Following ligation, the circularized probe is amplified, producing multiple copies of the gene-specific barcode for each target. Tissue slides were then stained using the 10x Genomics Multimodal Cell Segmentation Kit. During Multimodal staining, antibodies used for cell segmentation bind their antigens in an overnight incubation, followed by post-incubation washes to remove excess antibodies. The Multimodal Cell Segmentation kit stains for cell nuclei, membranes, and cell interior that are inputs for the 10x Genomics automated morphology-based cell segmentation analysis pipeline. Prepared tissue slides were then loaded for imaging on the Xenium Analyzer for in situ analysis. Fluorescently labeled oligos bind to the amplified DNA probes. Cyclical rounds of fluorescent probe hybridization, imaging, and removal generated optical patterns specific for each barcode, which were converted into a gene identity. Identified transcripts were then visualized using Xenium Explorer software.

Fig. S1. Trial study schema

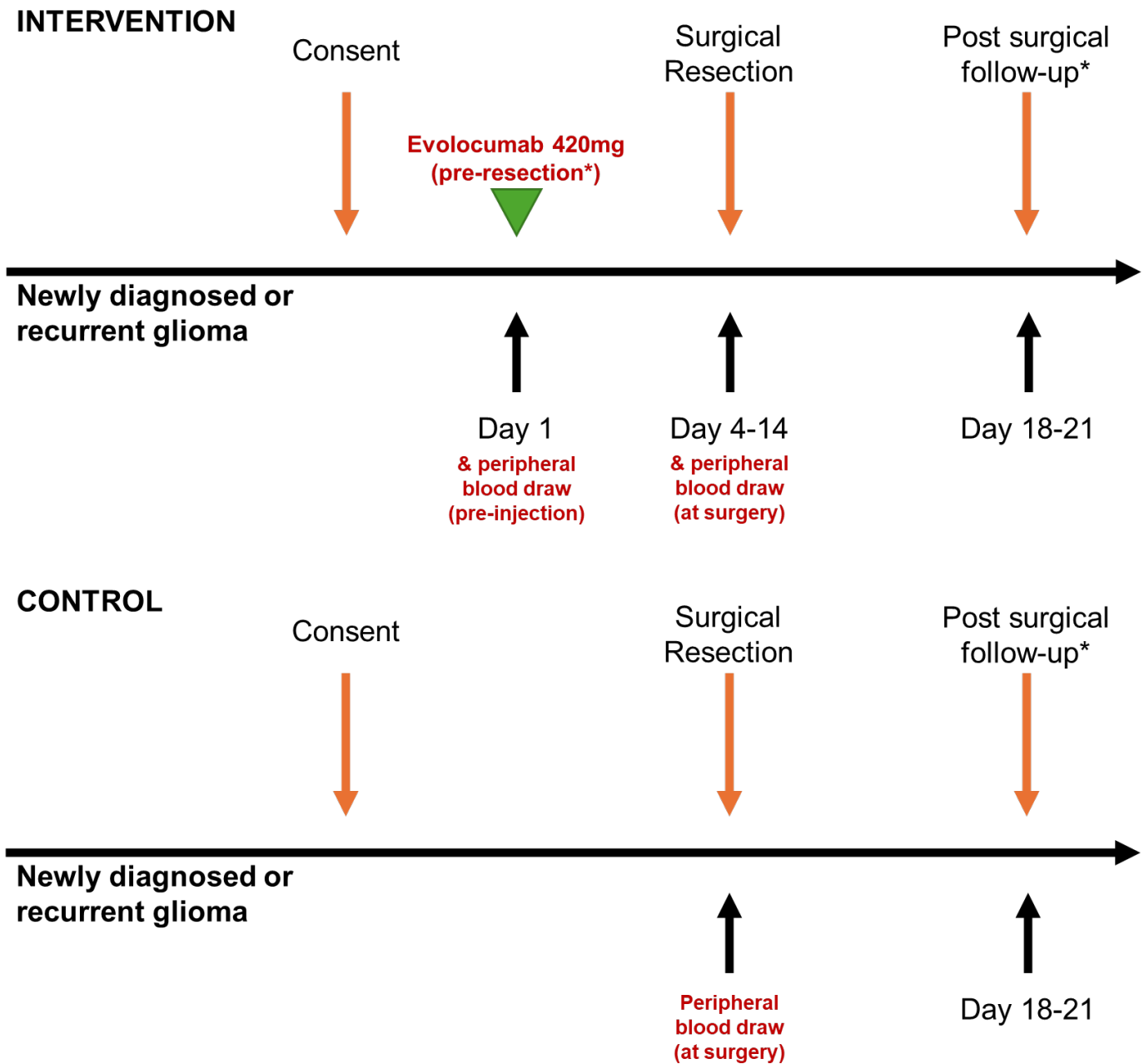
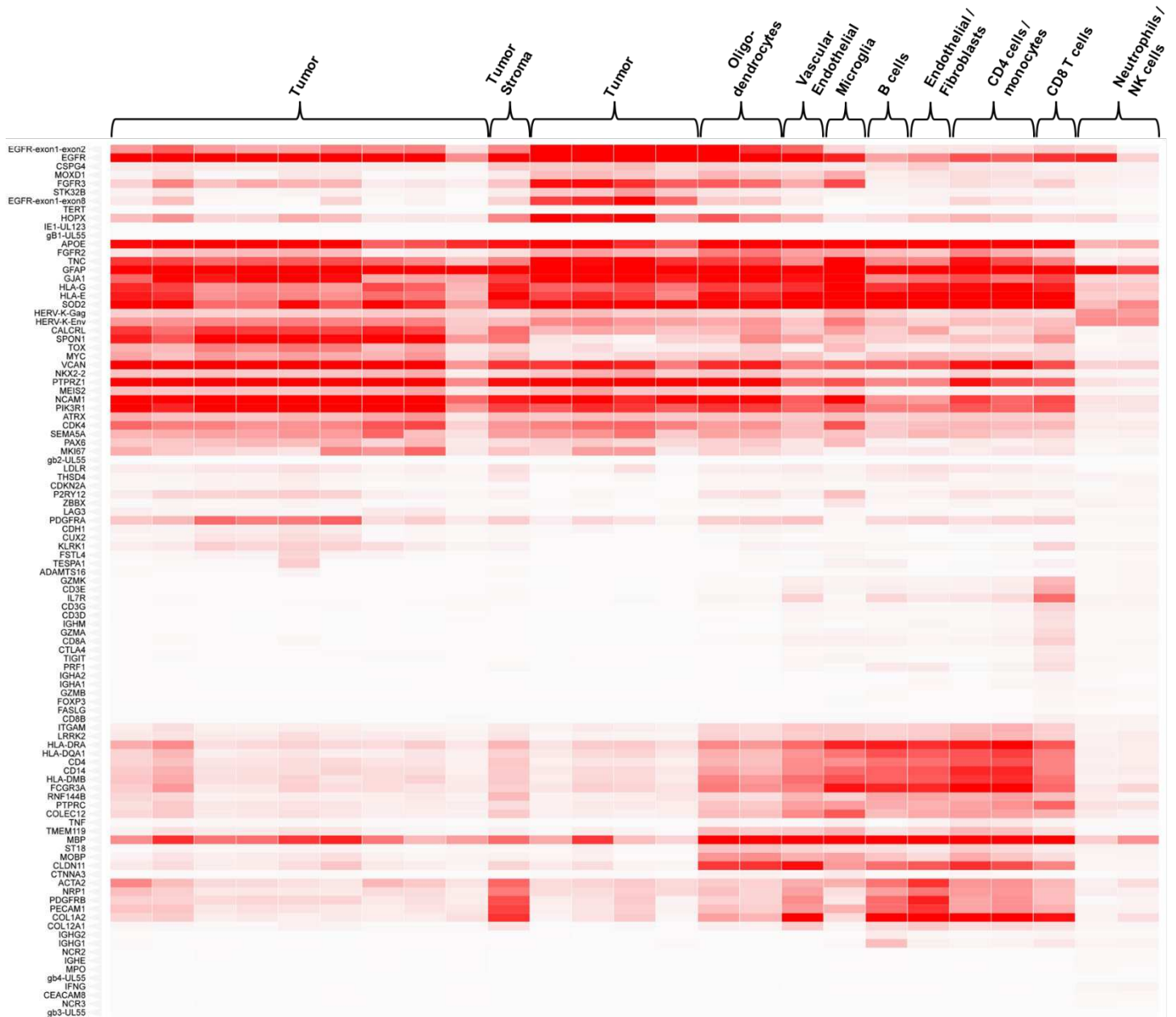
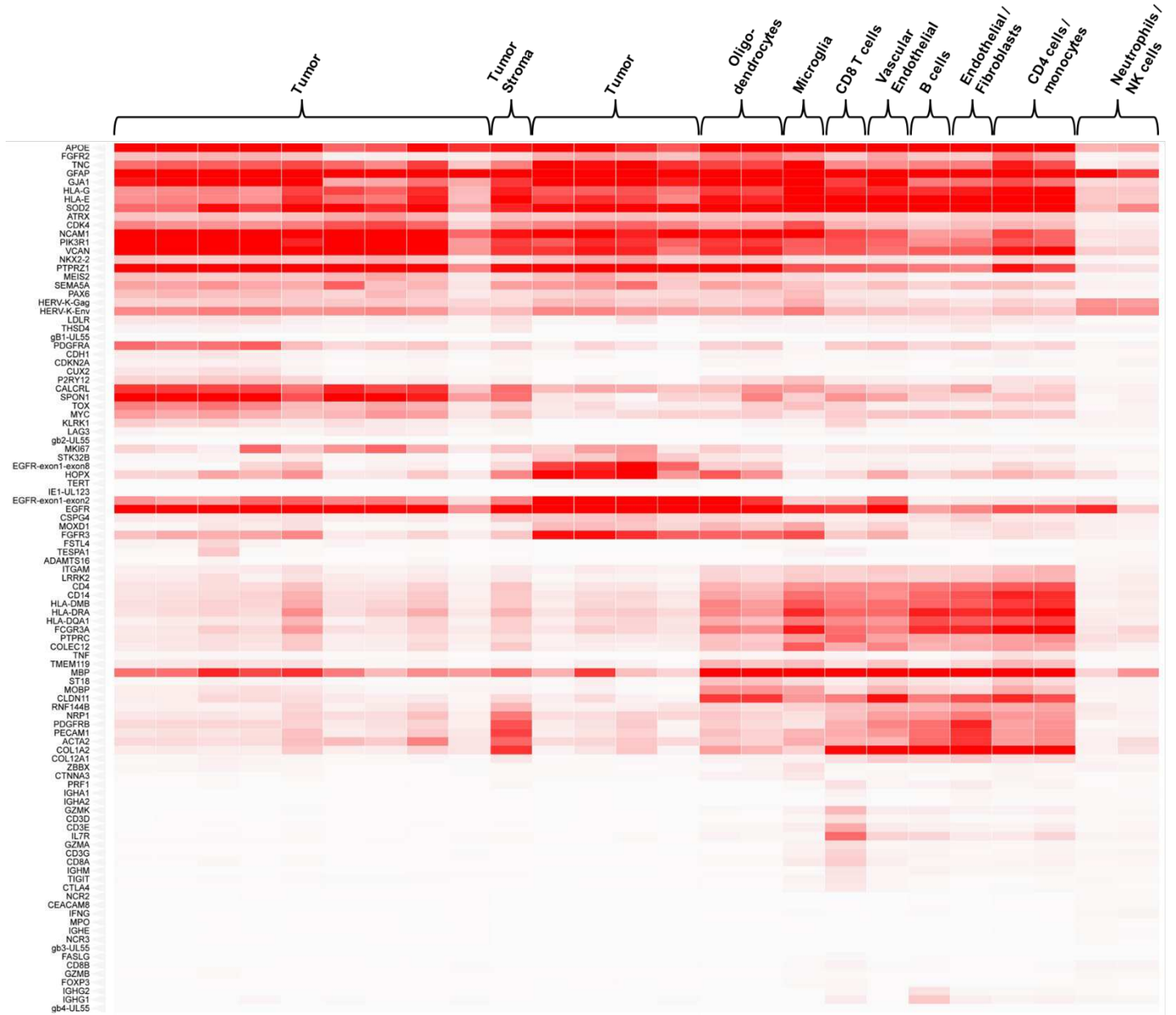


**Fig. S2. Clustering heatmap for grade IV gliomas**



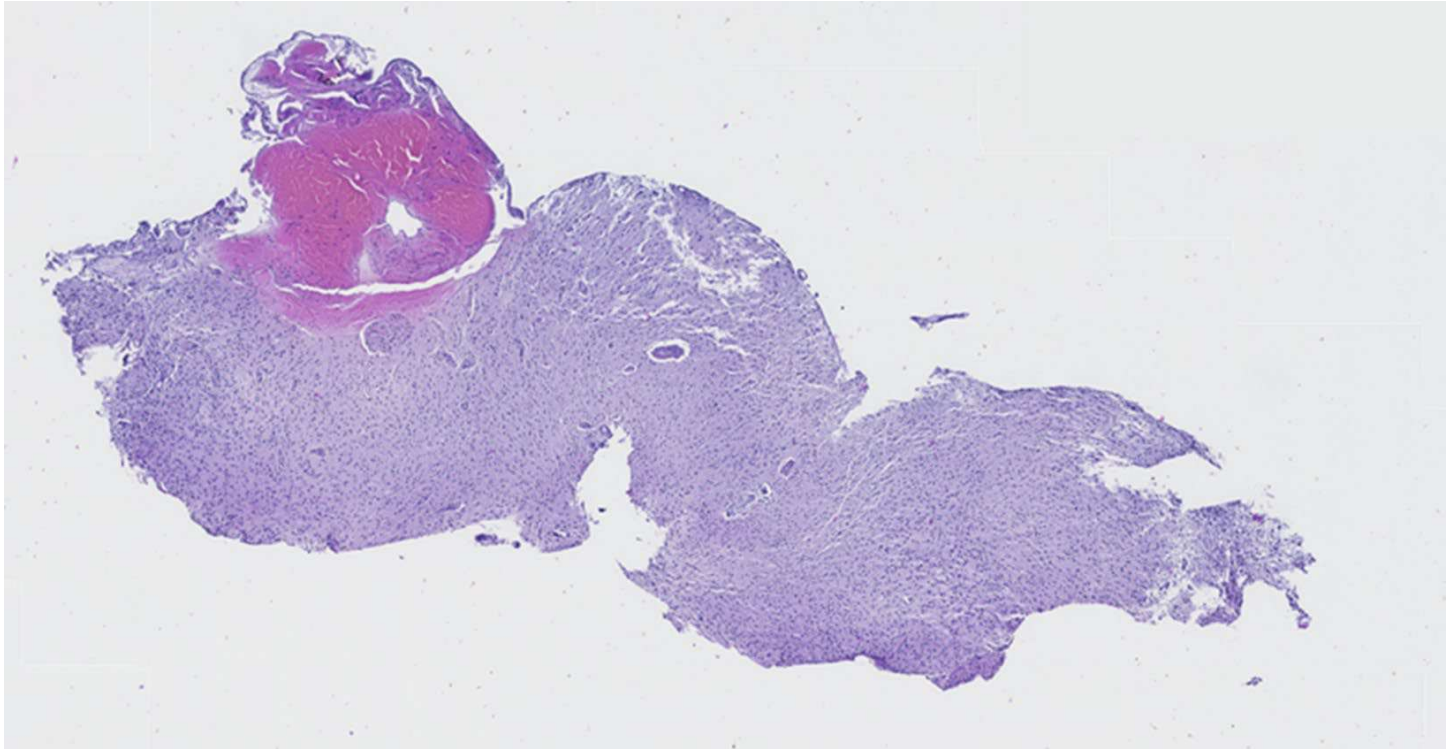
Hierarchical cluster heatmaps of gene transcripts from grade IV glioma samples shown, identifying regions of tumor, tumor stroma, oligodendrocytes, vascular endothelial cells, microglia, B cells, endothelial cells/fibroblasts, CD4 cells/monocytes, neutrophils/NK cells. Heatmaps generated using clustergrammer (Maayan Lab)

**Fig. S3. Clustering heatmap for grade II/III gliomas**



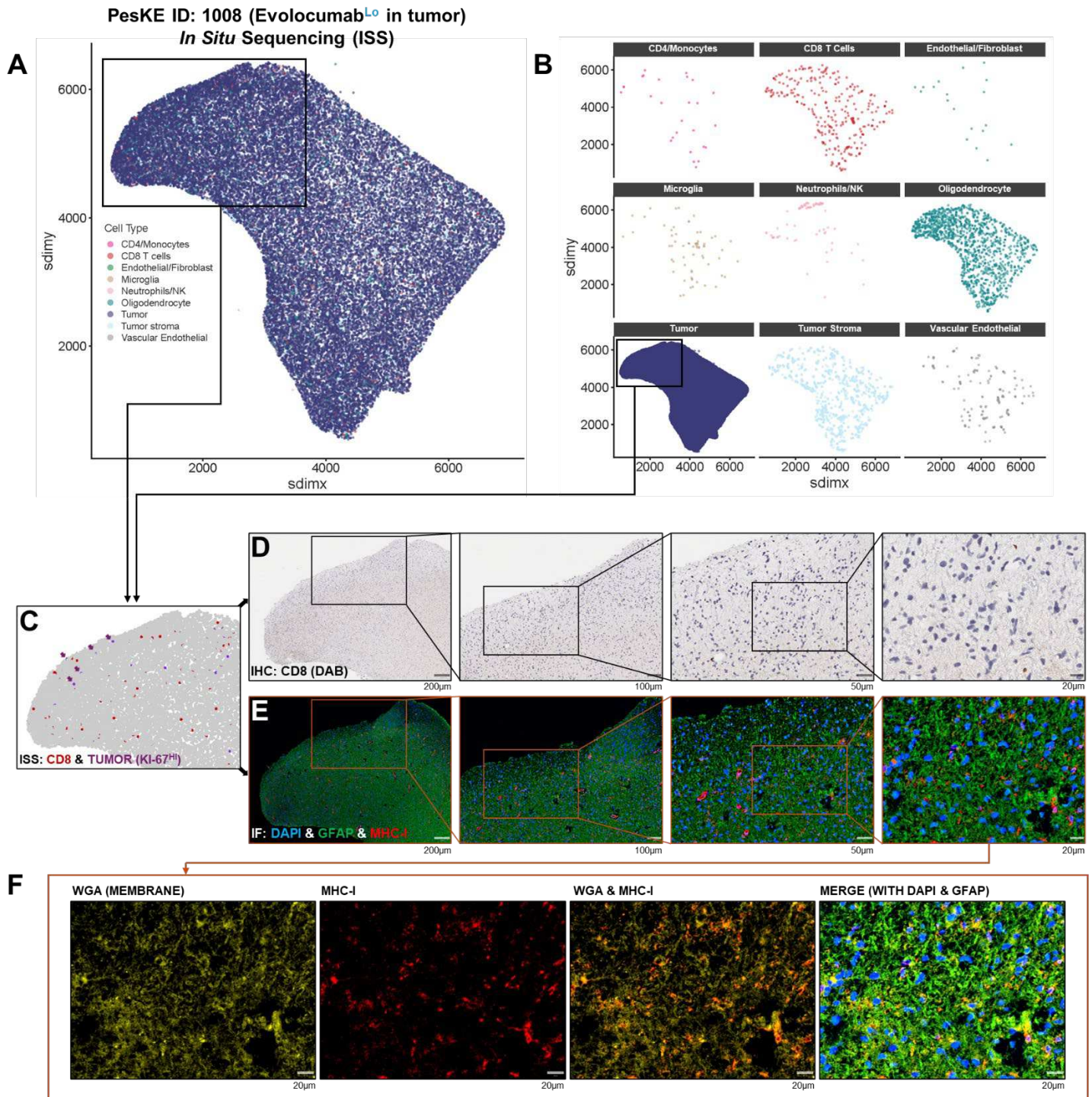
Hierarchical cluster heatmaps of gene transcripts from grade II/III glioma samples shown, identifying regions of tumor, tumor stroma, oligodendrocytes, microglia, CD8 T cells, vascular endothelial cells, B cells, endothelial cells/fibroblasts, CD4 cells/monocytes, neutrophils/NK cells. Heatmaps generated using clustergrammer (Maayan Lab)

**Fig. S4. H&E staining for grade IV tumor with high evolocumab uptake (ID: 1007)**



H&E sectioning of grade IV glioblastoma with high evolocumab uptake used in paired spatial RNA sequencing/IHC/IF staining (ID: 1007, 20x magnification shown)

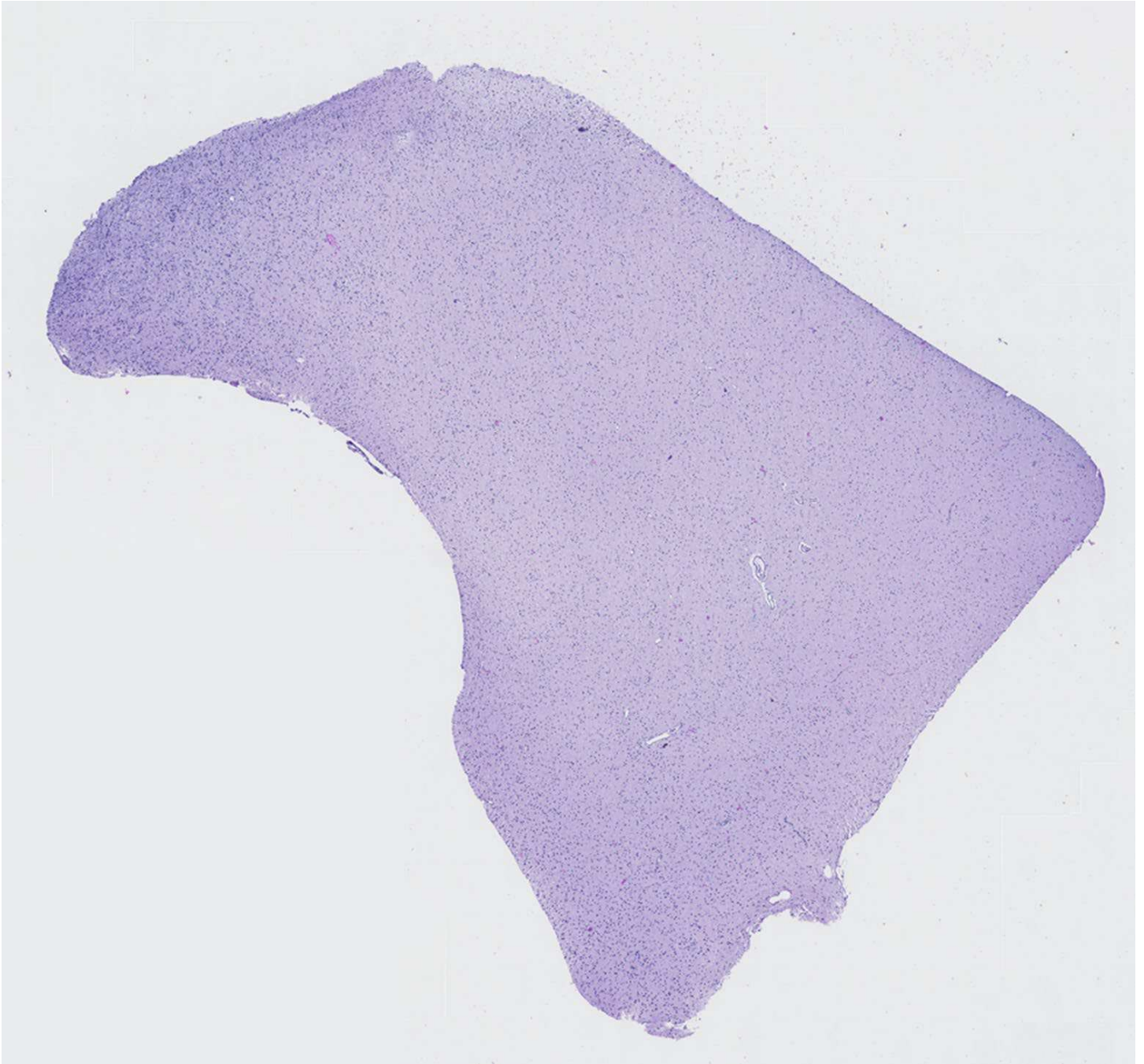
**Fig. S5. Paired spatial RNaseq/IHC/IF for grade II tumor with low evolocumab uptake (ID: 1008)**



(A-C) Paired *in situ* spatial RNA sequencing via Xenium platform and individual niches shown. Purple arrows in (C) identify proliferating tumor cells (Ki-67<sup>Hi</sup>), overlapping with a denser region of tumor assessed via H&E. CD8<sup>+</sup> T cells are highlighted in red.

(C-E) Paired Immunohistochemistry (IHC) and Immunofluorescence (IF) from tissue samples from a case with low evolocumab uptake (ID: 1008, grade II astrocytoma). Low levels CD8<sup>+</sup> infiltration within the parenchyma are observed on IHC. IF staining of GFAP (green), DAPI (nuclei, blue) and MHC-I (red) shows no obvious increase in MHC-I expression or co-localization with cell membranes (shown via WGA (yellow)).

**Fig. S6. H&E staining for grade II tumor with low evolocumab uptake (ID: 1008)**



H&E sectioning of grade II astrocytoma with low evolocumab uptake used in paired spatial RNA sequencing/IHC/IF staining (ID: 1008). The greatest intensity of staining is in the upper left-hand portion of tissue and migrates along the left-hand margin, typical of Grade 2 astrocytoma. 20x magnification shown.

**Table S1. Full inclusion & exclusion criteria for study**

Inclusion Criteria	Exclusion Criteria
<b>Both arms:</b>	<b>Treatment arm only:</b>
1. Adult patients $\geq 18$ years old	1. Any patient with a history of a serious hypersensitivity reaction to evolocumab or any of the excipients in evolocumab
2. Newly diagnosed glioma (diagnosis can be based on imaging) or recurrent glioma (if recurrent, prior pathology report demonstrating glioma is required)	2. Patients with severe hepatic impairment outside of the range defined in the inclusion criteria within 7 days of starting evolocumab.
3. A clinical indication for gross macroscopic resection, debulking of the glioma, or biopsy, with sufficient tumor size that can allow collection of specimens for the required analyses.	3. History or evidence of central nervous system bleeding as defined by stroke or intraocular bleed (including embolic stroke) not associated with any antitumor surgery within 6 months before enrollment
<b>Treatment arm only:</b>	4. Infection requiring intravenous antibiotics that was completed $< 1$ week of study enrollment (day 1) with the exemption of prophylactic antibiotics for long line insertion or biopsy
4. Adequate hematologic function within 14 days prior to starting evolocumab defined as follows: a. Hemoglobin $\geq 10$ g/dL ( <i>Note: the use of transfusion or other intervention to achieve Hgb <math>\geq 10.0</math> g/dl is acceptable</i> ) b. White Blood Cells $\geq 1.5 \times 10^9/L$ c. Absolute Neutrophil Count (ANC) $\geq 1.0 \times 10^9/L$ d. Platelets $\geq 100 \times 10^9/L$ or $\geq 50,000$ for patients who received TMZ within the past year	5. Females of reproductive potential and males who are unwilling to practice an acceptable method(s) of effective birth control while on study through 1 month (2 half-lives) after receiving the last dose of study drug.
5. Adequate renal function within 14 days prior to starting evolocumab defined as calculated creatinine clearance (CrCL) of $\geq 30$ mL/min/1.73m <sup>2</sup> by the Cockcroft-Gault formula	
6. Adequate hepatic function within 14 days prior to starting evolocumab defined as follows: a. Total bilirubin $\geq 1.5$ x institutional upper limit of normal (ULN) ( <i>Note: Patients with known Gilbert disease without other clinically significant liver abnormalities are not excluded.</i> ) b. AST(SGOT) and ALT(SGPT) $\geq 1.5 \times$ ULN	
7. Negative serum pregnancy test (in females of childbearing potential) within 48 hours of starting evolocumab.	

**Table S2. Demographics of consented participants**

<b>Age at Consent</b>	<b>N</b>	<b>Mean</b>	<b>Std Dev</b>	<b>Min</b>	<b>Median</b>	<b>Max</b>
Control	26	51.85	16.07	28.00	49.00	79.00
Evolocumab	6	53.00	19.88	28.00	52.00	74.00
	<b>Study Group</b>				<b>Total</b>	
	<b>Control</b>		<b>Evolocumab</b>			
	<b>N</b>	<b>%</b>	<b>N</b>	<b>%</b>		
<b>Gender</b>						
Male	12	46.15	4	66.67	16	50.00
Female	14	53.85	2	33.33	16	50.00
<b>Ethnicity</b>						
Not Hispanic or Latino	25	96.15	6	100.00	31	96.88
Unknown	1	3.85	0	0.00	1	3.13
<b>Race</b>						
White	22	84.62	6	100.00	28	87.50
Black or African American	3	11.54	0	0.00	3	9.38
Unknown	1	3.85	0	0.00	1	3.13
American Indian or Alaska Native	0	0.00	0	0.00	0	0.00
Asian	0	0.00	0	0.00	0	0.00
Native Hawaiian or other Pacific Islander	0	0.00	0	0.00	0	0.00
Not Reported	0	0.00	0	0.00	0	0.00
Multi-Race	0	0.00	0	0.00	0	0.00
<b>Histologic Grade</b>						
4	18	69.23	2	33.33	20	62.50
Not Applicable	6	23.08	2	33.33	8	25.00
No tumor tissue analysis	0	0.00	2	33.33	2	6.25
3	2	7.69	0	0.00	2	6.25
<b>Surgical Pathology Diagnosis of Analyzed Sample</b>						
Glioblastoma	17	65.38	2	33.33	19	59.38
Oligodendroglioma	3	11.54	1	16.67	4	12.50
No tumor tissue analysis	0	0.00	2	33.33	2	6.25
High Grade Astrocytoma, NOS	2	7.69	0	0.00	2	6.25
Low grade astrocytoma, NOS	0	0.00	1	16.67	1	3.13
Fibrillary Astrocytoma	1	3.85	0	0.00	1	3.13

Other, specify: High grade glioma	1	3.85	0	0.00	1	3.13
Anaplastic Astrocytoma	1	3.85	0	0.00	1	3.13
Diffuse Astrocytoma	1	3.85	0	0.00	1	3.13
<b>Disease Status</b>						
Newly Diagnosed	16	61.54	1	16.67	17	53.13
Previously Treated with Recurrent Disease	9	34.62	3	50.00	12	37.50
No tumor tissue analysis	0	0.00	2	33.33	2	6.25
Low grade treated, transformed	1	3.85	0	0.00	1	3.13
<b>Disease Description</b>						
Unifocal	24	92.31	4	66.67	28	87.50
No tumor tissue analysis	0	0.00	2	33.33	2	6.25
Multifocal	1	3.85	0	0.00	1	3.13
Unknown	1	3.85	0	0.00	1	3.13
<b>Site of Surgical Pathology Tumor</b>						
Frontal lobe	10	38.46	1	16.67	11	34.38
Temporal lobe	8	30.77	0	0.00	8	25.00
Parietal lobe	5	19.23	0	0.00	5	15.63
No tumor tissue analysis	0	0.00	2	33.33	2	6.25
Frontal-Parietal	1	3.85	1	16.67	2	6.25
Temporal-Occipital	0	0.00	1	16.67	1	3.13
Frontal-Temporal	0	0.00	1	16.67	1	3.13
Insula	1	3.85	0	0.00	1	3.13
Parietal-Temporal	1	3.85	0	0.00	1	3.13
<b>Total</b>	<b>26</b>	<b>100.00</b>	<b>6</b>	<b>100.00</b>	<b>32</b>	<b>100.00</b>

\*NOTE: Although 6 patients enrolled in the evolocumab group, only 4 had both tumor tissue and blood collected on study.

**Table S3. Toxicity summary of all Adverse Events among participants treated with evolocumab**

	Grade of Adverse Event					Treated Total N					
	1- Mild		2- Mod		3-Severe		4-LifeThr		5-Lethal		
	n	(%)	n	(%)	n		(%)	n	(%)	n	(%)
<b>Non-Hematologic Adverse Events</b>											
<b>GASTROINTESTINAL DISORDERS</b>											
Gastritis	0	(0%)	1	(17%)	0	(0%)	0	(0%)	0	(0%)	6
<b>GENERAL DISORDERS AND ADMINISTRATION SITE CONDITIONS</b>											
Injection site reaction	2	(33%)	0	(0%)	0	(0%)	0	(0%)	0	(0%)	6
<b>INFECTIONS AND INFESTATIONS</b>											
Thrush	1	(17%)	0	(0%)	0	(0%)	0	(0%)	0	(0%)	6
<b>METABOLISM AND NUTRITION DISORDERS</b>											
Dehydration	1	(17%)	0	(0%)	0	(0%)	0	(0%)	0	(0%)	6
<b>NERVOUS SYSTEM DISORDERS</b>											
Seizure	1	(17%)	0	(0%)	0	(0%)	0	(0%)	0	(0%)	6
<b>Non-Hematologic Adverse Events</b>											
Summary											
<b>Maximum Non-Hematologic AE</b>	<b>4</b>	<b>(67%)</b>	<b>1</b>	<b>(17%)</b>	<b>0</b>	<b>(0%)</b>	<b>0</b>	<b>(0%)</b>	<b>0</b>	<b>(0%)</b>	<b>6</b>
<b>All Adverse Events</b>											
Summary											
<b>Maximum Overall AE</b>	<b>4</b>	<b>(67%)</b>	<b>1</b>	<b>(17%)</b>	<b>0</b>	<b>(0%)</b>	<b>0</b>	<b>(0%)</b>	<b>0</b>	<b>(0%)</b>	<b>6</b>

**Table S4. Toxicity summary of Adverse Events among participants possibly, probably, or definitely related to evolocumab**

	Grade of Adverse Event					Treated Total N			
	1- Mild		2- Mod		3-Severe		4-LifeThr	5-Lethal	
	n	(%)	n	(%)	n		(%)	n	(%)
<b>Non-Hematologic Adverse Events</b>									
GENERAL DISORDERS AND ADMINISTRATION SITE CONDITIONS									
Injection site reaction	2	(33%)	0	(0%)	0	(0%)	0	(0%)	6
<b>Non-Hematologic Adverse Events</b>									
Summary									
Maximum Non-Hematologic AE	2	(33%)	0	(0%)	0	(0%)	0	(0%)	6
<b>All Adverse Events</b>									
Summary									
Maximum Overall AE	2	(33%)	0	(0%)	0	(0%)	0	(0%)	6